

Set-membership target search and tracking with cooperating UAVs using vision systems

Maxime Zagar^{1,2}, Luc Meyer², Michel Kieffer¹, Hélène Piet-Lahanier²

Abstract

This paper addresses the problem of target search and tracking using a fleet of cooperating UAVs evolving in some unknown region of interest containing an *a priori* unknown number of moving ground targets. Each UAV is equipped with an embedded Computer Vision System (CVS), providing an image with labeled pixels and a depth map of the observed part of its environment. Moreover, when a target is identified, a box containing the corresponding pixels in the image is also provided. Hypotheses regarding information related to the classified pixels, the depth map, and the boxes are introduced to allow its exploitation by set-membership approaches. Using information provided by the CVS and these hypotheses, each UAV evaluates sets guaranteed to contain the location of the identified targets and a set containing the possible locations of targets still to be identified. Then, each UAV uses these sets to design its trajectory to search and track targets. The efficiency of the proposed approach is illustrated via simulations.

I. INTRODUCTION

The problem of searching and tracking targets using a fleet of Unmanned Aerial Vehicles (UAVs) in some Region of Interest (RoI) has attracted considerable attention in recent years, see, *e.g.*, [1]–[4] and the references therein. The difficulty of this problem depends (i) on the knowledge available on the environment and on whether it is structured or not, (ii) on the type and quality of information provided by the sensors embedded in the UAVs, and (iii) on the *a priori* knowledge about targets (shape, number, dynamics).

Cooperative Search, Acquisition, and Track (CSAT) problems in possibly unknown and cluttered environments are still challenging [4]. In absence of prior knowledge, a representation of the environment is usually constructed in parallel to the search for targets [5], [6] using techniques such as those presented in [7]. For that purpose, UAVs must be equipped with a Computer Vision System (CVS) including a camera and image processing algorithms. Many prior works assume that a UAV gets a noisy measurement of the state of targets present in its Field of View (FoV) [8]–[12]. The complex processing performed by the CVS to get the state measurement from data acquired by the camera is usually ignored. As a consequence, the estimation uncertainty associated to the state measurements is difficult to characterize, and is thus roughly approximated, which is a major limit of those approaches.

This work has been submitted to the Elsevier / ScienceDirect for possible publication. Copyright may be transferred without notice, after which this version may no longer be accessible.

¹ Université Paris-Saclay, CentraleSupélec, CNRS, L2S, 91192 Gif-sur-Yvette, France `first_name.last_name@l2s.centralesupelec.fr`

² DTIS, ONERA Université Paris-Saclay, Palaiseau, France `first_name.last_name @ onera.fr`

This paper presents a CSAT approach for ground targets evolving in a structured environment for which no prior map is available. UAVs embed a CVS consisting of a camera with a limited FoV, a pixel classifier, a depth map evaluation algorithm, and a target detection algorithm. Hypotheses are introduced regarding the information obtained from these algorithms to facilitate its processing by the UAVs. A distributed set-membership estimation approach is proposed to exploit the CVS information so as to obtain sets containing the locations of identified targets compliant with the considered hypotheses. A set containing all locations of targets still to be identified is also evaluated. CVS information is also exploited to build sets where there is no target. Each UAV exploits the information provided by its own CVS and then accounts for the information broadcast by its neighbors. The trajectory of each UAV of the fleet is then evaluated using a variant of the Model Predictive Control (MPC) of [13] so as to minimize the overall estimation uncertainty characterized by the size of the set estimates.

To the best of our knowledge, this paper presents the first approach to address a CSAT problem by a distributed set-membership approach exploiting directly CVS information. Its main contributions lie (i) in the introduction of hypotheses to exploit the information provided by the CVS in a set-membership context, (ii) in the proposition of the associated set-membership estimation approach, and (iii) in the consideration of an unknown structured environment where obstacles may hide targets. The performance of the proposed approach is evaluated via a simulation in a simplified urban environment.

Section II reviews some related work. The CSAT problem is formulated in Section III after a description of models for the targets and the UAVs. Section IV introduces models and hypotheses related to the information collected by the CVS so that it may be exploited in a set-membership context. The set-membership estimator is detailed in Section V and in Section VI. Section VII briefly summarizes the distributed MPC approach to design the trajectory of each UAV. Simulation results are provided in Section VIII. Section IX concludes the paper and provides some perspectives.

II. RELATED WORKS

CSAT approaches using a fleet of UAVs require finding, identifying, locating, and tracking an unknown number of targets in some RoI [2], [4]. This necessitates collecting measurements allowing to discriminate the zones where a target can be located from the zones free of targets. When a target has been identified and its location estimated, the UAVs must keep track of its displacements while pursuing the exploration of the RoI. Therefore, the trajectories of the UAVs result in a compromise between exploratory search and target tracking. Many approaches have been proposed to achieve parts of these various goals, fewer address all of them, especially in an unknown environment.

A. Representation of the RoI

The simplest description of ROI is a cuboid or a simple geometric shape without obstacle. In this context, search trajectories for a fleet of UAVs have been designed in [14]–[16]. Nevertheless, the efficiency of these approaches decreases in presence of occlusions due to obstacles, leading to possible non-detections.

To account for the presence of obstacles, the fleet of UAVs may either exploit some *a priori* known map of the environment or build a map during the exploration. Exploration in cluttered environment without any map has been

considered in [17], where a swarm of robots is driven to a target emitting some signal while using an obstacle collision avoidance approach. When several possibly partly hidden targets have to be found, [11] considers groups of UAVs, each observing a part of the RoI with complementary points of view. This limits the risk of a target being occluded from all points of view and does not require building a map of the environment. The price to be paid is an increase of the size of the fleet. Using a known map, the UAV trajectories can be efficiently determined [9], [18], [19]. Occlusions of the FoV by obstacles may be taken into account, as in [20], [21].

Many Simultaneous Localization and Mapping (SLAM) algorithms have been developed to build maps, see the survey [7]. The map may be represented by an occupancy grid [22], an OcTree [23], or a point cloud [24]. The availability of semantic information improves the mapping algorithms [23], [25]–[28], for example to distinguish static and mobile objects as in [26]. In outdoor environment mapping, [27], [28] use semantic information to evaluate the *traversability* between two locations, *i.e.*, the possibility to reach one location from another. Nevertheless, 3D mapping and exploration of large outdoor environments is still challenging [7], especially for aerial vehicles due to their limited computational power. For example, the mapping of a city-scale environment with an occupancy grid raises storage issues. OcTree mapping may reduce this complexity as shown in [23], but their study is limited to a ground exploration of areas of $150 \text{ m} \times 150 \text{ m}$.

CSAT algorithms including map construction during exploration have been considered in [5], [6]. These approaches consider either a 2D [6] or a 3D [5] description of the RoI, but neglect potential occlusions of the FoV by obstacles in the trajectory design.

B. Environment perception and target detection

Environment exploration, target detection, and map building heavily rely on the information provided by the UAV sensors, such as images provided by cameras or depth measurements obtained either from LiDARs, or by processing the acquired images [29]–[32]. Several computer vision algorithm may then be exploited such as image or point cloud segmentation [33]–[35]. Target detection techniques [36]–[39] may then be put at work.

Once a target has been detected, several approaches have been proposed to estimate its location. In [18], [40]–[44], images of an RGB camera are used to estimate the location of a target in a reference frame from its location in the images. These approaches exploit a specific pixel, generally belonging to a 2D bounding box containing the pixels associated to the target. The selection of the pixel most representative of the target location is often heuristic and may lead to relatively large localization errors, as evidenced in [45] when estimating the location of humans evolving in the overlapping FoVs of static cameras. In [46], images of ArUco markers with known positions are acquired by UAVs, processed by a CVS, and exploited by a set-membership approach to cooperatively estimate the pose of the UAVs. Deep learning techniques are now commonly used for target location estimation. For example, YOLO [36] is used to localize a human in an unknown environment present in the FoV of a UAV in [47]. When the target remains in the FoV, it is tracked via optical-flow techniques. In [48], YOLO exploits RGB images and depth information to detect and localize ArUco markers placed on objects. Using strong *a priori* information such as 3D models of the target shapes, deep learning algorithms exploiting images and depth information, are able to estimate

the location and orientation of static objects [25], [49], or vehicles [50], [51]. Nevertheless, these algorithms may provide erroneous estimates with errors difficult to characterize [52].

C. Estimates of a target location

To represent the estimated target locations, a probability map is often considered, which requires a spatial discretization of the RoI [19], [53]. Nevertheless, the performance of grid-based approaches heavily relies on the choice of the cell dimension, and extension to large RoI is an issue [7]. Alternative approaches such as [14], [16] combine a probability hypothesis density filter and random finite sets. Assuming a bounded measurement noise, set-membership techniques may be used as in [13] to get sets guaranteed to contain the actual locations of targets, provided that the hypotheses on the noise bounds are satisfied.

Determining parts of RoI free of targets may be very helpful in the exploration process to reduce the estimation uncertainty of target locations. The absence or presence of a target within an area monitored by a UAV depends on the capacity of the embedded CVS to detect the presence of a target [54], often represented by a probability of detection. Nevertheless, this probability is highly dependent on the observation conditions (UAV point of view, possible occlusions) as evidenced in [55] and [20]. As its characterization is difficult, it is used in many approaches [5], [14], [15], [54], but most often without justification. Alternatively, deterministic, point-of-view dependent, target detection conditions have been introduced in [11]. A target may be detected and identified only when it is observed from some set of point of views. The set of point of views may be deduced from a map of the environment, as in [21]. Alternatively, the UAVs may be organized to observe simultaneously parts of the RoI from a large variety of point of views [11].

D. Trade-off between exploration and tracking

When mobile targets outnumber the UAVs, it proves difficult to maintain constant monitoring of the detected targets. Different approaches have been proposed to trade off environment exploration and target tracking. Pre-planned trajectories are used in [56], [57]. In [20], several next best viewpoints for each UAV are first identified using the approach of [22], [58]. Then, polynomial trajectories are designed passing through these viewpoints while avoiding known obstacles. A potential-field based path-planning approach is developed in [5] to reach a location in a 3D cluttered environment. The goal location is a cell characterized by a higher uncertainty about the presence of a target than other cells. In [14], each UAV updates its trajectory with new weighted center of Voronoi cells obtained once the random finite sets describing the possible target locations are updated. Trajectories are designed in [12], [15], [47] via reinforcement learning techniques. A MPC approach is used in [13] to design UAV trajectories minimizing the predicted estimation uncertainty corresponding to the area of the set estimates related to identified targets and of the set still to be explored.

III. MODELS AND PROBLEM FORMULATION

Consider an urban environment to which a frame \mathcal{F} is attached. The RoI $\mathbb{X}_0 \subset \mathbb{R}^2 \times \mathbb{R}^+$ is a subset of the environment and its ground \mathbb{X}_g is assumed to be flat, *i.e.*, $\mathbb{X}_g = \{\mathbf{x} \in \mathbb{X}_0 \mid x_3 = 0\}$, x_3 being the altitude of

\mathbf{x} . N^o static obstacles are spread within \mathbb{X}_0 , with N^o unknown. The shape \mathbb{S}_m^o of the by the m -th obstacle, $m \in \mathcal{N}^o = \{1, \dots, N^o\}$, is the part of \mathbb{X}_0 it occupies. \mathbb{S}_m^o is unknown but for all $m \in \mathcal{N}^o$, but we assume that

$$\forall \mathbf{x} \in \mathbb{S}_m^o, \forall \lambda \in [0, 1], \lambda \mathbf{x} + (1 - \lambda) \mathbf{p}_g(\mathbf{x}) \in \mathbb{S}_m^o, \quad (1)$$

where $\mathbf{p}_g(\mathbf{x})$ is the projection of \mathbf{x} on the ground \mathbb{X}_g . The assumption (1) is consistent with the representation of buildings by a pyramidal stack of parallelipeds introduced by [24].

A fleet of N^u UAVs with indexes in the set $\mathcal{N}^u = \{1, \dots, N^u\}$ is deployed in the RoI. The UAVs search a fixed but unknown number N^t of ground targets with indexes in the set $\mathcal{N}^t = \{1, \dots, N^t\}$. We assume that the targets never leave \mathbb{X}_0 nor enter in any obstacle.

Sections III-A and III-B introduce the models and assumptions considered for targets and UAVs. Then Section III-C formalizes the CSAT problem. In what follows, the time is sampled with a period T and k refers to the time index. Several frames are introduced, such as the frames attached to a UAV and to its camera. To lighten the notations, vectors with no superscript related to a frame are implicitly expressed in \mathcal{F} .

A. Target model

At time $t_k = kT$, the state of target $j \in \mathcal{N}^t$ is $\mathbf{x}_{j,k}^t$. The vector $\mathbf{x}_{j,k}^t$ containing the first three components of $\mathbf{x}_{j,k}^t$ gathers the coordinates of the center of gravity of target j . The projection $\mathbf{x}_{j,k}^{t,g} = \mathbf{p}_g(\mathbf{x}_{j,k}^t)$ of $\mathbf{x}_{j,k}^t$ on \mathbb{X}_g represents the target location at time t_k . It is assumed to evolve as

$$\mathbf{x}_{j,k+1}^{t,g} = \mathbf{f}^t(\mathbf{x}_{j,k}^{t,g}, \mathbf{v}_{j,k}^t), \quad (2)$$

where \mathbf{f}^t is known and $\mathbf{v}_{j,k}^t$ is some unknown target control input only assumed to belong to a known box $[v^t]$. The space occupied by target j is the subset $\mathbb{S}_j^t(\mathbf{x}_{j,k}^t)$ of \mathbb{X}_0 and depends on $\mathbf{x}_{j,k}^t$. When the target shape is rigid, *e.g.*, for cars, $\mathbb{S}_j^t(\mathbf{x}_{j,k}^t)$ depends mainly on the target position and orientation. We assume that

$$\mathbf{x}_{j,k}^t \in \mathbb{S}_j^t(\mathbf{x}_{j,k}^t). \quad (3)$$

The target location $\mathbf{x}_{j,k}^{t,g}$, however, does not necessarily belong to $\mathbb{S}_j^t(\mathbf{x}_{j,k}^t)$, as in the case of cars, for example.

Usually, the type of targets to be localized is known. Consequently, some information about the target dimensions is available. We assume that for any target state $\mathbf{x}_{j,k}^t$

$$\mathbb{S}_j^t(\mathbf{x}_{j,k}^t) \subset \mathbb{C}^t(\mathbf{x}_{j,k}^{t,g}), \quad (4)$$

where $\mathbb{C}^t(\mathbf{x}_{j,k}^{t,g})$ is a vertical circular right cylinder of known height h^t and radius r^t with basis centered in $\mathbf{x}_{j,k}^{t,g}$. The projection $\mathbf{p}_g(\mathbb{C}^t(\mathbf{x}_{j,k}^{t,g}))$ of $\mathbb{C}^t(\mathbf{x}_{j,k}^{t,g})$ on \mathbb{X}_g is the disc $\mathbb{D}_g(\mathbf{x}_{j,k}^{t,g}, r^t)$ of center $\mathbf{x}_{j,k}^{t,g}$ and radius r^t included in \mathbb{X}_g .

We assume that targets cannot enter in any obstacle, *i.e.*,

$$\forall j \in \mathcal{N}^t, \forall m \in \mathcal{N}^o, \mathbb{S}_{j,k}^t(\mathbf{x}_{j,k}^t) \cap \mathbb{S}_m^o = \emptyset. \quad (5)$$

Consider the r -neighborhood of a set $\mathbb{S} \subset \mathbb{X}_0$ as

$$\mathbb{N}(\mathbb{S}, r) = \{\mathbf{x} \in \mathbb{X}_0 \mid d(\mathbf{x}, \mathbb{S}) \leq r\} \quad (6)$$

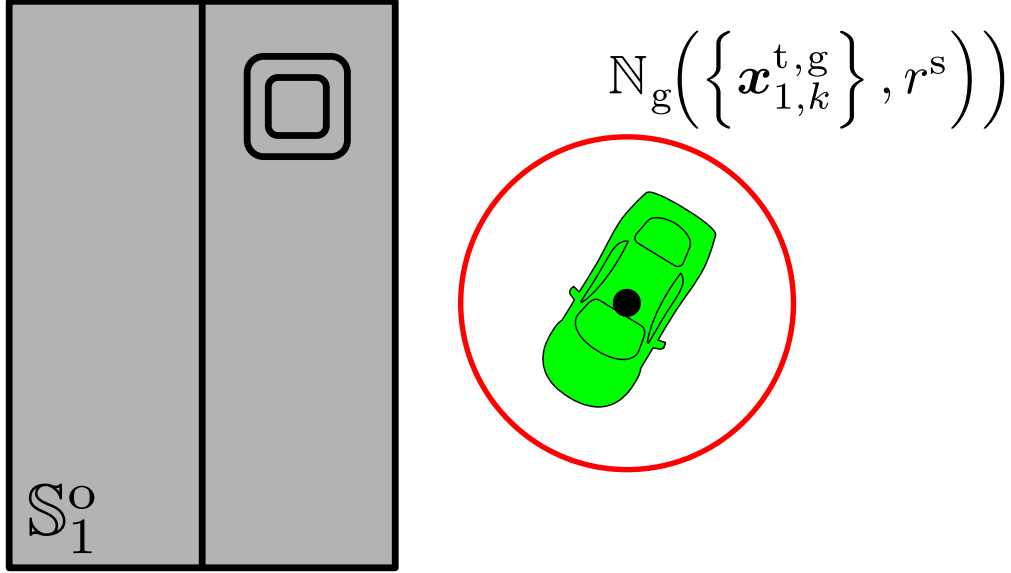


Figure 1. Obstacle (in grey), target (in green), and r^s -ground neighborhood (in red) of its location.

with $d(\mathbf{x}, \mathbb{S}) = \min_{\mathbf{y} \in \mathbb{S}} \|\mathbf{x} - \mathbf{y}\|$ and the r -ground neighborhood of the projection on the ground of a set $\mathbb{S} \subset \mathbb{X}_0$ defined as

$$\mathbb{N}_g(\mathbb{S}, r) = \{\mathbf{x} \in \mathbb{X}_g \mid d(\mathbf{x}, \mathbf{p}_g(\mathbb{S})) \leq r\}. \quad (7)$$

We assume further that the target location $\mathbf{x}_{j,k}^{t,g}$ remains at a distance strictly larger than some known safety distance $r^s \geq r^t$ of any obstacle \mathbb{S}_m^o , i.e., that

$$\forall j \in \mathcal{N}^t, \forall m \in \mathcal{N}^o, d(\mathbf{x}_{j,k}^{t,g}, \mathbb{S}_m^o) > r^s. \quad (8)$$

From (1), one has $\mathbf{p}_g(\mathbb{S}_m^o) \subset \mathbb{S}_m^o$. Consequently, (8) implies that

$$\forall j \in \mathcal{N}^t, \forall m \in \mathcal{N}^o, \mathbb{N}_g(\{\mathbf{x}_{j,k}^{t,g}\}, r^s) \cap \mathbf{p}_g(\mathbb{S}_m^o) = \emptyset, \quad (9)$$

see Figure 1.

B. UAV model

At time t_k , the state vector $\mathbf{x}_{i,k}^u$ of UAV $i \in \mathcal{N}^u$ contains, among others, the location of its center of gravity $\mathbf{x}_{i,k}^u \in \mathbb{R}^2 \times \mathbb{R}^{+*}$. The space occupied by UAV i is $\mathbb{S}^u(\mathbf{x}_{i,k}^u)$. Its dynamic is modeled as

$$\mathbf{x}_{i,k+1}^u = \mathbf{f}^u(\mathbf{x}_{i,k}^u, \mathbf{u}_{i,k}^u), \quad (10)$$

where \mathbf{f}^u is known and the control input $\mathbf{u}_{i,k}^u$ is constrained within a bounded set \mathbb{U} . The state $\mathbf{x}_{i,k}^u$ is assumed to be perfectly known by UAV i .

Each UAV is equipped by a camera and a CVS. In addition to the acquired image $\mathbf{I}_{i,k}$ at time t_k , the CVS provides a depth-map $\mathbf{D}_{i,k}$ obtained using, e.g., [29], [31], [32], an array of pixel labels $\mathbf{L}_{i,k}$ obtained using, e.g., [33], [34], and a list $\mathcal{D}_{i,k}^t$ of identified targets. For each $j \in \mathcal{D}_{i,k}^t$, a box $\left[\mathcal{Y}_{i,j,k}^t\right]$ in the image $\mathbf{I}_{i,k}$ containing pixels

of each identified target is provided, *e.g.*, by [36]–[39]. These boxes are gathered in a list $\mathcal{B}_{i,k}^t = \left\{ \left[\mathcal{Y}_{i,j,k}^t \right] \right\}_{j \in \mathcal{D}_{i,k}^t}$. We assume that $\mathbf{D}_{i,k}$ and $\mathbf{L}_{i,k}$ have the same size as $\mathbf{I}_{i,k}$.

The communications within the fleet are modeled by the undirected graph $\mathcal{G}_k = (\mathcal{N}^u, \mathcal{E}_k)$, with \mathcal{N}^u the set of vertices and $\mathcal{E}_k = \mathcal{N}^u \times \mathcal{N}^u$ the set of edges of the graph. \mathcal{E}_k describes the connectivity at time t_k . For two UAVs $i \in \mathcal{N}^u$ and $i' \in \mathcal{N}^u$, if $(i, i') \in \mathcal{E}_k$, then both UAVs are able to exchange information without delay and error. The set $\mathcal{N}_{i,k} = \{i' \in \mathcal{N}^u \mid (i, i') \in \mathcal{E}_k\}$ contains all UAV indexes with which UAV i is able to communicate at time t_k . We consider that $i \in \mathcal{N}_{i,k}$.

C. Problem formulation

The information available to UAV i before time t_k is gathered in the set $\mathcal{I}_{i,k-1}$. $\mathcal{I}_{i,k-1}$ contains, among others, a list $\mathcal{L}_{i,k-1}^t$ of indexes of targets already identified. For each $j \in \mathcal{L}_{i,k-1}^t$, we assume that UAV i has access to a set estimate $\mathbb{X}_{i,j,k-1}^t \subset \mathbb{X}_g$ of all possible target locations $\mathbf{x}_{j,k-1}^{t,g}$ which are consistent with $\mathcal{I}_{i,k-1}$. It has also access to a set $\bar{\mathbb{X}}_{i,k-1}^t$ containing all locations where targets still to be detected may be present.

Using the information collected by the camera and processed by the CVS at time t_k , the information available at time t_k to UAV i is then $\mathcal{I}_{i,k|k} = \mathcal{I}_{i,k-1} \cup \left\{ \mathbf{I}_{i,k}, \mathbf{D}_{i,k}, \mathbf{L}_{i,k}, \mathcal{D}_{i,k}^t, \mathcal{B}_{i,k}^t \right\}$. With this information UAV i evaluates an updated list of identified targets $\mathcal{L}_{i,k|k}^t = \mathcal{L}_{i,k-1}^t \cup \mathcal{D}_{i,k}^t$. UAV i has then, for each target $j \in \mathcal{L}_{i,k|k}^t$, to characterize the set $\mathbb{X}_{i,j,k|k}^t \subset \mathbb{X}_g$ of all possible target locations $\mathbf{x}_{j,k}^{t,g}$ which are consistent with $\mathcal{I}_{i,k|k}$. UAV i has also to update the estimate $\bar{\mathbb{X}}_{i,k-1}^t$ to get $\bar{\mathbb{X}}_{i,k|k}^t$.

Then, UAV i broadcasts some updated information to its neighbors $\mathcal{N}_{i,k}$ and receives information from them. The type of information exchanged is detailed in Section VI-C. After communication, the total information UAV i has now access to is denoted $\mathcal{I}_{i,k}$. UAV i can then further update its list of identified targets to get $\mathcal{L}_{i,k}^t$, the set estimates $\mathbb{X}_{i,j,k}^t$ for each $j \in \mathcal{L}_{i,k}^t$ gathered in the set $\mathcal{X}_{i,k}^t = \left\{ \mathbb{X}_{i,j,k}^t \right\}_{j \in \mathcal{L}_{i,k}^t}$, and evaluate an updated version of $\bar{\mathbb{X}}_{i,k|k}^t$ denoted $\bar{\mathbb{X}}_{i,k}^t$.

The target localization uncertainty is defined as

$$\Phi \left(\mathcal{X}_{i,k}^t, \bar{\mathbb{X}}_{i,k}^t \right) = \phi \left(\bar{\mathbb{X}}_{i,k}^t \cup \bigcup_{j \in \mathcal{L}_{i,k}^t} \mathbb{X}_{i,j,k}^t \right), \quad (11)$$

where $\phi(\mathbb{X})$ is the area of the set $\mathbb{X} \subset \mathbb{R}^2$. $\Phi \left(\mathcal{X}_{i,k}^t, \bar{\mathbb{X}}_{i,k}^t \right)$ account for already identified and still to be identified targets.

Our aim in what follows is (i) to show the way set estimates are obtained from CVS information, (ii) to determine the type of information to be exchanged between UAVs, (iii) to present the way set estimates are updated using $\mathcal{I}_{i,k}^N$, and (iv) to design the trajectory of each UAV so as to minimize (11).

IV. HYPOTHESES ON THE CVS

In this section, some hypotheses are introduced to exploit the information provided by the CVS using set-membership estimation techniques. Section IV-A presents a geometrical model for the camera embedded in UAVs. Then, Section IV-B introduces hypotheses related to CVS information. Section IV-C presents an assumption on the light rays illuminating the CCD array when the location of a target is in the FoV of an UAV. In the remainder of this section, the time index k is omitted to lighten the notations.

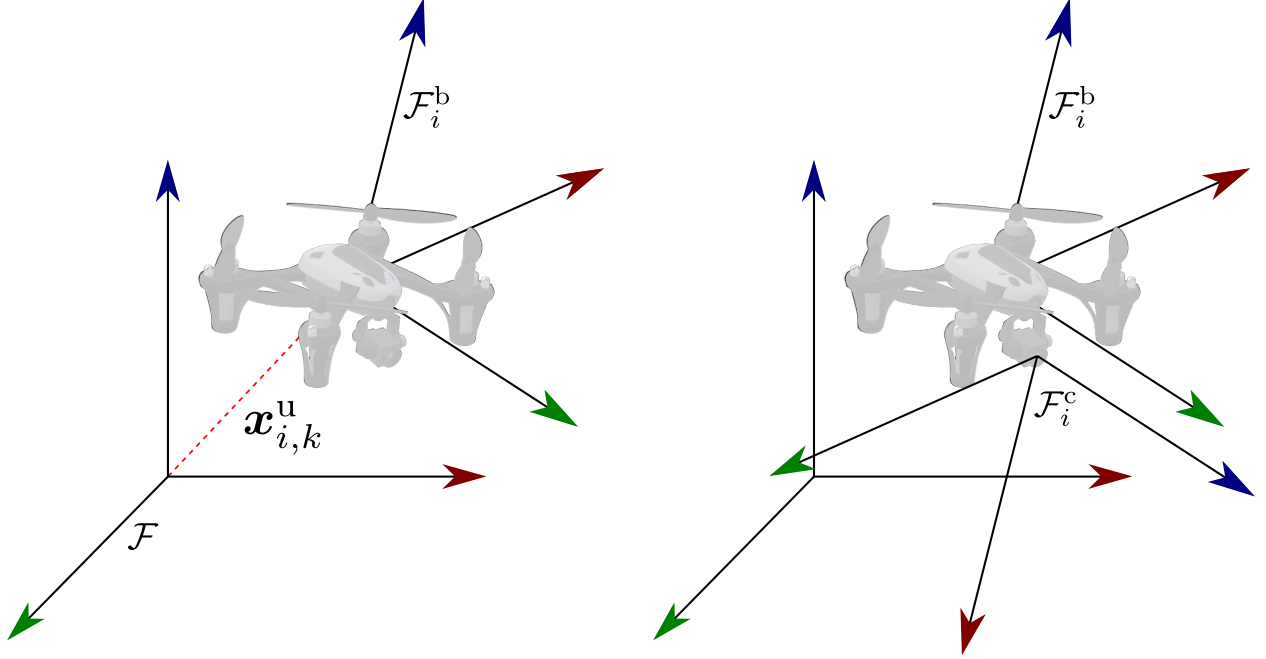


Figure 2. Left: Reference frame \mathcal{F} and UAV body frame \mathcal{F}_i^b ; Right: Camera frame \mathcal{F}_i^c and body frame \mathcal{F}_i^b of UAV i , when $\theta = 0$

A. Camera model and field of view

A body frame \mathcal{F}_i^b , illustrated in Figure 2, with origin $\mathbf{x}_{i,k}^u$ is attached to UAV i . The rotation matrix from \mathcal{F} to \mathcal{F}_i^b is denoted $\mathbf{M}_{\mathcal{F}}^{\mathcal{F}_i^b}$. $\mathbf{M}_{\mathcal{F}}^{\mathcal{F}_i^b}$ depends on $\mathbf{x}_{i,k}^u$. The coordinates of some vector $\mathbf{x} \in \mathbb{R}^3$ in \mathcal{F} , when expressed in \mathcal{F}_i^b , are

$$\mathbf{T}_{\mathcal{F}}^{\mathcal{F}_i^b}(\mathbf{x}) = \mathbf{M}_{\mathcal{F}}^{\mathcal{F}_i^b}(\mathbf{x} - \mathbf{x}_{i,k}^u). \quad (12)$$

Each UAV i of the fleet embeds the same type of CCD camera which provides an image \mathbf{I}_i of N_r rows and N_c columns. The camera frame \mathcal{F}_i^c of UAV i has its optical center $\mathbf{x}_{i,k}^{\mathcal{F}_i^c}$ as origin and is oriented such that the positive z -axis represents the optical axis of the camera. The x -axis is parallel to the pixel rows in the CCD array and the y -axis is parallel to the columns. The rotation matrix from \mathcal{F}_i^b to \mathcal{F}_i^c is

$$\mathbf{M}_{\mathcal{F}_i^b}^{\mathcal{F}_i^c} = \begin{pmatrix} 0 & -1 & 0 \\ 0 & 0 & -1 \\ 1 & 0 & 0 \end{pmatrix} \begin{pmatrix} \cos \theta & 0 & -\sin \theta \\ 0 & 1 & 0 \\ \sin \theta & 0 & \cos \theta \end{pmatrix}, \quad (13)$$

where θ is the fixed camera angle between the x -axis of \mathcal{F}_i^b and the z -axis of \mathcal{F}_i^c . Figure 2 illustrates these two frames.

The dimensions $H_r \times H_c$ of the CCD array of the camera and its focal length f are known. A pinhole model without distortion [59] is considered for the camera. Therefore, the matrix of intrinsic parameters [59] used to project a point of \mathcal{F}_i^c onto the CCD array is

$$\mathbf{K} = \begin{pmatrix} -f_c & 0 & N_c/2 \\ 0 & -f_r & N_r/2 \end{pmatrix} \quad (14)$$

where $f_c = fN_c/H_c$ and $f_r = fN_r/H_r$ are the focal lengths expressed in pixels. Consequently, the 2D coordinates on the CCD array of the projection of some point $\mathbf{x}^{\mathcal{F}_i^c} \in \mathbb{R}^3$ are

$$\mathbf{p}_{\mathcal{F}_i^c}(\mathbf{x}^{\mathcal{F}_i^c}) = \mathbf{K}\mathbf{x}^{\mathcal{F}_i^c}/x_3^{\mathcal{F}_i^c}. \quad (15)$$

According to the considered pinhole model, each light ray passing through the optical center of the camera and illuminating the CCD array at $(x, y) \in [0, N_c] \times [0, N_r]$ can be modeled by a half-line of direction

$$\mathbf{v}^{\mathcal{F}_i^c}(x, y) = \frac{1}{\nu(x, y)} \begin{pmatrix} (N_c/2 - x)/f_c \\ (N_r/2 - y)/f_r \\ 1 \end{pmatrix}, \quad (16)$$

with $\nu(x, y) = \sqrt{((N_c/2 - x)/f_c)^2 + ((N_r/2 - y)/f_r)^2 + 1}$. The set

$$\mathcal{V}_i(n_r, n_c) = \left\{ \mathbf{M}_{\mathcal{F}_i^c}^{\mathcal{F}} \mathbf{v}^{\mathcal{F}_i^c}(x, y) \mid x \in [n_c - 1, n_c], y \in [n_r - 1, n_r] \right\}, \quad (17)$$

with $\mathbf{M}_{\mathcal{F}_i^c}^{\mathcal{F}} = \mathbf{M}_{\mathcal{F}_i^b}^{\mathcal{F}} \mathbf{M}_{\mathcal{F}_i^c}^{\mathcal{F}_i^b}$, contains the directions, expressed in \mathcal{F} , of all light rays contributing to the illumination of the pixel (n_r, n_c) .

The FoV $\mathbb{F}(\mathbf{x}_i^u)$ of the CCD camera of UAV i (dubbed as FoV of UAV i in what follows) represents the set of points in \mathbb{X}_0 that are potentially observed (ignoring obstacles and targets). $\mathbb{F}(\mathbf{x}_i^u)$ is a half-cone with the camera optical center \mathbf{x}_i^c as its apex and with four unit vectors $\mathbf{v}_\ell^{\mathcal{F}_i^c}$, $\ell = 1, \dots, 4$, describing its edges, *i.e.*,

$$\mathbb{F}(\mathbf{x}_i^u) = \left\{ \mathbf{x}_i^c + \sum_{\ell=1}^4 a_\ell \mathbf{M}_{\mathcal{F}_i^c}^{\mathcal{F}} \mathbf{v}_\ell^{\mathcal{F}_i^c} \mid a_\ell \in \mathbb{R}^+ \right\}. \quad (18)$$

These four unit vectors can be deduced from (16) by taking (x, y) at the four corners of the CCD array. In what follows, we assume that any information related to some $\mathbf{x} \in \mathbb{F}(\mathbf{x}_i^u)$ at a distance from \mathbf{x}_i^c larger than d_{\max} cannot be considered as reliable. One introduces then the subset

$$\underline{\mathbb{F}}(\mathbf{x}_i^u) = \mathbb{F}(\mathbf{x}_i^u) \cap \mathbb{B}(\mathbf{x}_i^c, d_{\max}), \quad (19)$$

of the FoV where $\mathbb{B}(\mathbf{x}_i^c, d_{\max})$ is the ball of \mathbb{R}^3 of center \mathbf{x}_i^c and radius d_{\max} . $\underline{\mathbb{F}}(\mathbf{x}_i^u)$ contains all points of $\mathbb{F}(\mathbf{x}_i^u)$ at a distance from \mathbf{x}_i^c less than d_{\max} .

The coordinates of a point $\mathbf{x} \in \underline{\mathbb{F}}(\mathbf{x}_i^u)$, when expressed in \mathcal{F}_i^b are $\mathbf{x}^{\mathcal{F}_i^b} = \mathbf{T}_{\mathcal{F}}^{\mathcal{F}_i^b}(\mathbf{x}) \in \mathbb{R}^3$. To express them in \mathcal{F}_i^c , one evaluates

$$\mathbf{T}_{\mathcal{F}_i^c}^{\mathcal{F}_i^b}(\mathbf{x}^{\mathcal{F}_i^b}) = \mathbf{M}_{\mathcal{F}_i^c}^{\mathcal{F}_i^b}(\mathbf{x}^{\mathcal{F}_i^b} - \mathbf{x}_i^{c, \mathcal{F}_i^b}). \quad (20)$$

Composing (12) and (20), one gets the transform

$$\mathbf{T}_{\mathcal{F}}^{\mathcal{F}_i^c} = \mathbf{T}_{\mathcal{F}_i^c}^{\mathcal{F}_i^b} \circ \mathbf{T}_{\mathcal{F}}^{\mathcal{F}_i^b} \quad (21)$$

to express the coordinates of $\mathbf{x} \in \underline{\mathbb{F}}(\mathbf{x}_i^u)$ in \mathcal{F}_i^c . Combining (15) and (21), the coordinates of the image on the CCD array of a point $\mathbf{x} \in \underline{\mathbb{F}}(\mathbf{x}_i^u)$ are

$$\mathbf{p}_c(\mathbf{x}_i^u, \mathbf{x}) = \mathbf{p}_{\mathcal{F}_i^c}(\mathbf{T}_{\mathcal{F}}^{\mathcal{F}_i^c}(\mathbf{x})). \quad (22)$$

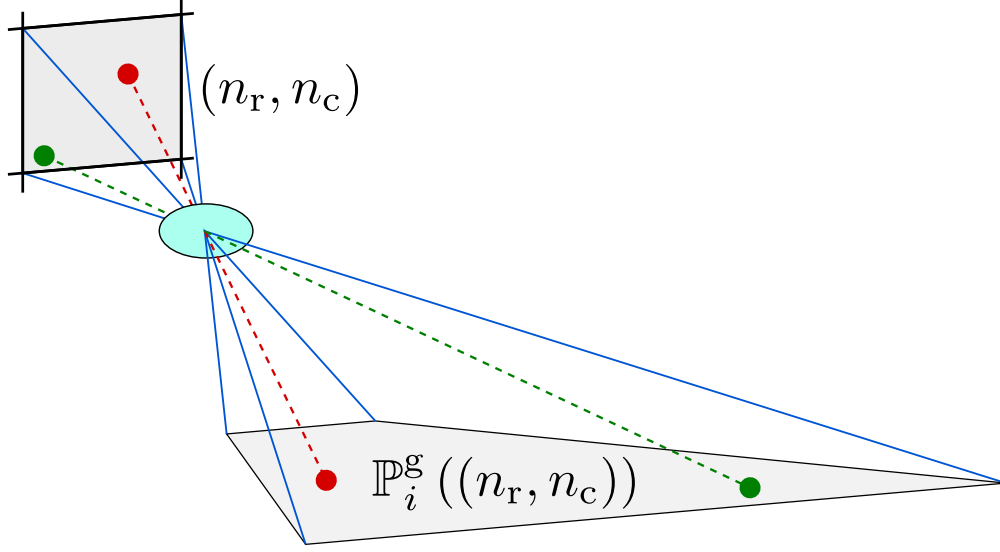


Figure 3. Pinhole model of the camera and several light rays contributing to the illumination of the pixel (n_r, n_c) ; The 4 blue lines are the light rays illuminating the corners of (n_r, n_c) ; The quadrangle $\mathbb{P}_i^g((n_r, n_c))$ represents all points of the ground which may contribute to the illumination of pixel (n_r, n_c) , see Section V.

The notation $p_c(\mathbf{x}_i^u, \mathbf{x}) \in (n_r, n_c)$, with $\mathbf{x} \in \mathbb{F}(\mathbf{x}_i^u)$, indicates that the projection of \mathbf{x} on the CCD array belongs to the pixel with coordinates $(n_r, n_c) \in \mathcal{N}^I$, with $\mathcal{N}^I = \{1 \dots N_r\} \times \{1 \dots N_c\}$. Consequently, one has

$$\mathbf{x} \in \mathbb{F}(\mathbf{x}_i^u) \Rightarrow \exists (n_r, n_c) \in \mathcal{N}^I, p_c(\mathbf{x}_i^u, \mathbf{x}) \in (n_r, n_c). \quad (23)$$

B. Exploiting information provided by the CVS

This section presents the assumptions considered to exploit the information provided by the CVS embedded in each UAV. Section IV-B1 introduces an assumption on the information in \mathbf{D}_i used to get bounded-error measurements of the distance from the camera to parts of the environment. Section IV-B2 presents assumptions on the pixel labels \mathbf{L}_i . Section IV-B3 introduces assumptions related to bounding boxes $[\mathcal{Y}_{i,j}^l], j \in \mathcal{D}_i$, and labeled pixels for targets identified by the CVS.

1) *From a depth map to bounded-error range measurements:* The distance between the optical center of the camera \mathbf{x}_i^c and the environment (including obstacles and targets) along $\mathbf{v} \in \mathcal{V}_i(n_r, n_c)$, for any $(n_r, n_c) \in \mathcal{N}^I$, is

$$\rho(\mathbf{x}_i^c, \mathbf{v}) = \min \left\{ d_v(\mathbf{x}_i^c, \mathbb{X}_g), d_v(\mathbf{x}_i^c, \bigcup_{m \in \mathcal{N}^o} \mathbb{S}_m^o), \right. \\ \left. d_v(\mathbf{x}_i^c, \bigcup_{j \in \mathcal{N}^l} \mathbb{S}_j^l(\mathbf{x}_j^l)), d_v(\mathbf{x}_i^c, \bigcup_{\ell \in \mathcal{N}^u} \mathbb{S}^u(\mathbf{x}_\ell^u)) \right\}, \quad (24)$$

where $d_v(\mathbf{x}, \mathbb{S})$ is the distance from a point $\mathbf{x} \in \mathbb{X}_0$ to the intersection of the set \mathbb{S} along the half-line of origin \mathbf{x} and direction \mathbf{v} . Then

$$\rho(\mathbf{x}_i^c, \mathcal{V}_i(n_r, n_c)) = \{\rho(\mathbf{x}_i^c, \mathbf{v}) \mid \mathbf{v} \in \mathcal{V}_i(n_r, n_c)\}, \quad (25)$$

is the set of all distances between \mathbf{x}_i^c and the environment along any direction $\mathbf{v} \in \mathcal{V}_i(n_r, n_c)$.

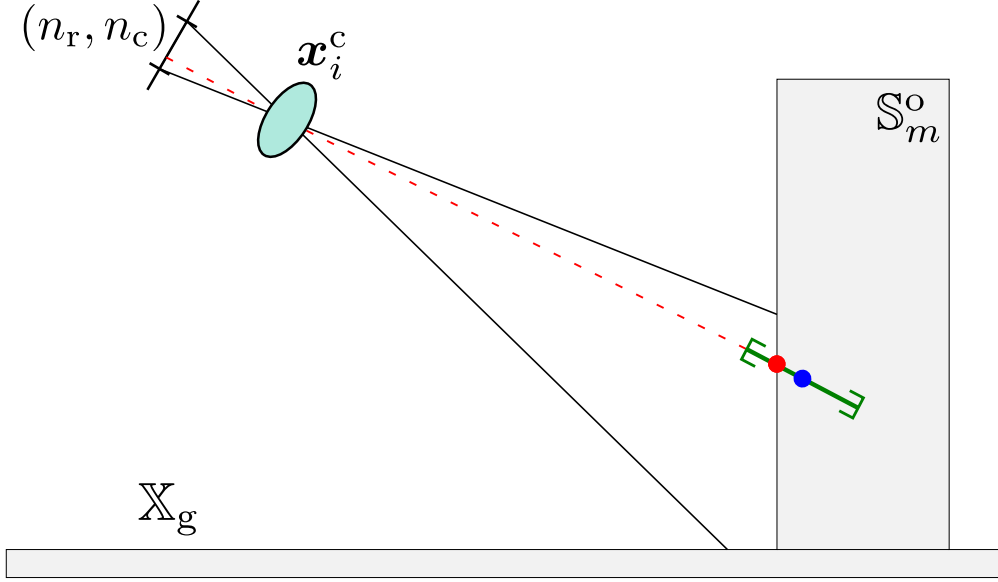


Figure 4. Depth map information for one pixel: $\mathbf{D}_i^0(n_r, n_c)$ is the distance between \mathbf{x}_i^c and the red dot, while $\mathbf{D}_i(n_r, n_c)$ represents the measured distance between \mathbf{x}_i^c and the blue dot; The green interval is $[\mathbf{D}_i](n_r, n_c)$.

We assume that each element $\mathbf{D}_i(n_r, n_c)$ of the depth map is a noisy version

$$\mathbf{D}_i(n_r, n_c) = \mathbf{D}_i^0(n_r, n_c) (1 + w) \quad (26)$$

of the distance $\mathbf{D}_i^0(n_r, n_c) = \rho(\mathbf{x}_i^c, \mathbf{v})$ between \mathbf{x}_i^c and the environment along some unknown direction $\mathbf{v} \in \mathcal{V}_i(n_r, n_c)$. In (26), the noise w is assumed to belong to the known interval $[\underline{w}, \overline{w}]$. Consequently, the interval

$$[\mathbf{D}_i](n_r, n_c) = [1/(1 + \overline{w}), 1/(1 + \underline{w})] \mathbf{D}_i(n_r, n_c). \quad (27)$$

contains $\mathbf{D}_i^0(n_r, n_c)$, see Figure 4.

2) *Pixel classification*: Each element (n_r, n_c) of the array of pixel labels \mathbf{L}_i is assumed to belong to one of the following classes: Ground, Target, Obstacle, and Unknown/Not Labeled. The latter class corresponds to pixels that cannot be classified in one of the three other classes due to a lack of confidence. According to (19), all information coming from a point that may not be in $\mathbb{F}(\mathbf{x}_i^u)$ is considered as unreliable. Therefore, using \mathbf{D}_i , one introduces the list of pixel coordinates

$$\mathcal{Y}_i = \left\{ (n_r, n_c) \in \mathcal{N}^I \mid \frac{1}{1 + \underline{w}} \mathbf{D}_i(n_r, n_c) \leq d_{\max} \right\} \quad (28)$$

for which reliable information is assumed available, especially about their labeling. All pixels with indexes in \mathcal{Y}_i are assumed to be correctly classified (possibly as Unknown, when there is an ambiguity).

Four subsets of \mathcal{Y}_i are then deduced from \mathbf{L}_i , namely \mathcal{Y}_i^g , \mathcal{Y}_i^t , \mathcal{Y}_i^o , and \mathcal{Y}_i^n gathering coordinates of pixels respectively labeled as Ground, Target, Obstacle, and Unknown/Not Labeled. We assume that pixels corresponding to other UAVs are labeled as Unknown. Moreover, we assume that if a pixel $(n_r, n_c) \in \mathcal{Y}_i^g$, then all light rays illuminating (n_r, n_c) stem from the ground \mathbb{X}_g , i.e.,

$$\forall \mathbf{v} \in \mathcal{V}_i(n_r, n_c), \rho(\mathbf{x}_i^c, \mathbf{v}) = d_v(\mathbf{x}_i^c, \mathbb{X}_g). \quad (29)$$

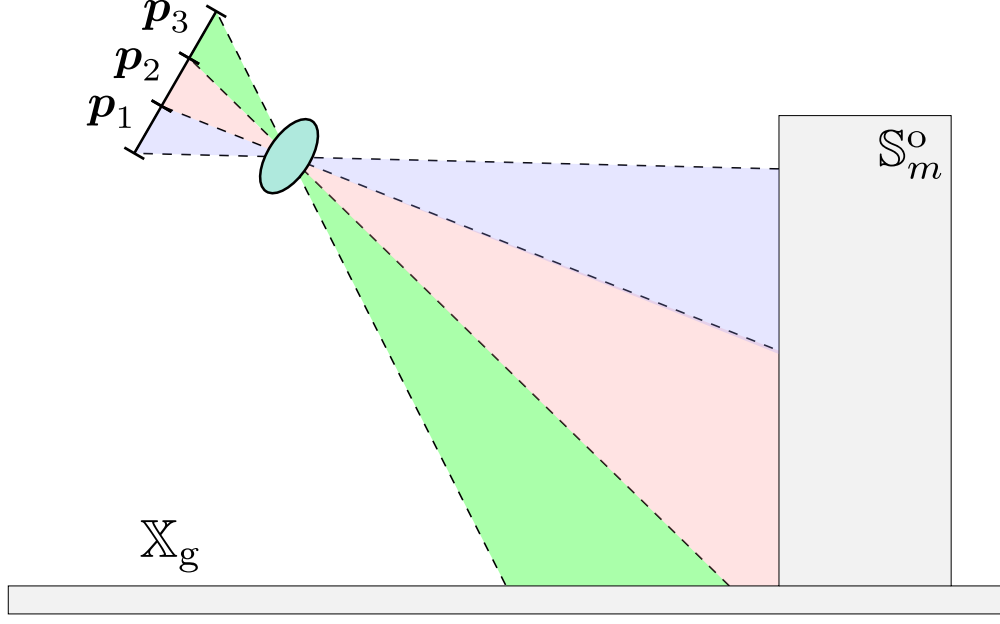


Figure 5. As pixel $p_1 \in \mathcal{Y}_i^o$, all light rays illuminating p_1 stem from an obstacle; as pixel $p_3 \in \mathcal{Y}_i^g$, all light rays illuminating p_3 stem from \mathbb{X}_g ; As $p_2 \in \mathcal{Y}_i^n$, nothing can be concluded.

Similarly, if a pixel $(n_r, n_c) \in \mathcal{Y}_i^t$, then there exists a target $j \in \mathcal{N}^t$ such that all light rays illuminating (n_r, n_c) stem from $\mathbb{S}_j^t(\mathbf{x}_{j,k}^t)$, i.e.,

$$\forall \mathbf{v} \in \mathcal{V}_i(n_r, n_c), \exists j \in \mathcal{N}^t, \rho(\mathbf{x}_i^c, \mathbf{v}) = d_{\mathbf{v}}(\mathbf{x}_i^c, \mathbb{S}_j^t(\mathbf{x}_{j,k}^t)). \quad (30)$$

Finally, if a pixel $(n_r, n_c) \in \mathcal{Y}_i^o$, then for all light rays illuminating (n_r, n_c) , there exists an obstacle $m \in \mathcal{N}^o$ such that the light ray stem from \mathbb{S}_m^o , i.e.,

$$\forall \mathbf{v} \in \mathcal{V}_i(n_r, n_c), \exists m \in \mathcal{N}^o, \rho(\mathbf{x}_i^c, \mathbf{v}) = d_{\mathbf{v}}(\mathbf{x}_i^c, \mathbb{S}_m^o). \quad (31)$$

See Figure 5.

3) *Bounding boxes for identified targets:* When \mathcal{Y}_i^t is not empty, at least one target located within $\mathbb{F}(\mathbf{x}_i^t)$ has been detected. In such case, the CVS may also provide a list $\mathcal{D}_i^t \subset \mathcal{N}^t$ of identified targets and an axis-aligned box $[\mathcal{Y}_{i,j}^t]$, for each $j \in \mathcal{D}_i^t$. \mathcal{D}_i^t may be empty even if \mathcal{Y}_i^t is not empty, when \mathcal{Y}_i^t does not contain enough information to identify a target.

Consider the set $\mathcal{Y}_{i,j}^t \subset \mathcal{Y}_i^t$ containing all pixels of \mathcal{Y}_i^t associated to target j only. If $j \in \mathcal{D}_i^t$, we assume that $\mathcal{Y}_{i,j}^t$ is not empty, i.e.,

$$j \in \mathcal{D}_i^t \Rightarrow \mathcal{Y}_{i,j}^t \neq \emptyset. \quad (32)$$

Moreover, the CVS is assumed to be tuned in such a way that $[\mathcal{Y}_{i,j}^t]$ contains $\mathcal{Y}_{i,j}^t$, i.e.,

$$j \in \mathcal{D}_i^t \Rightarrow \mathcal{Y}_{i,j}^t \subset [\mathcal{Y}_{i,j}^t]. \quad (33)$$

We assume further that the classifier is unable to provide $\mathcal{Y}_{i,j}^t$. Therefore, the target location estimator will have to exploit $[\mathcal{Y}_{i,j}^t]$ and \mathcal{Y}_i^t only.

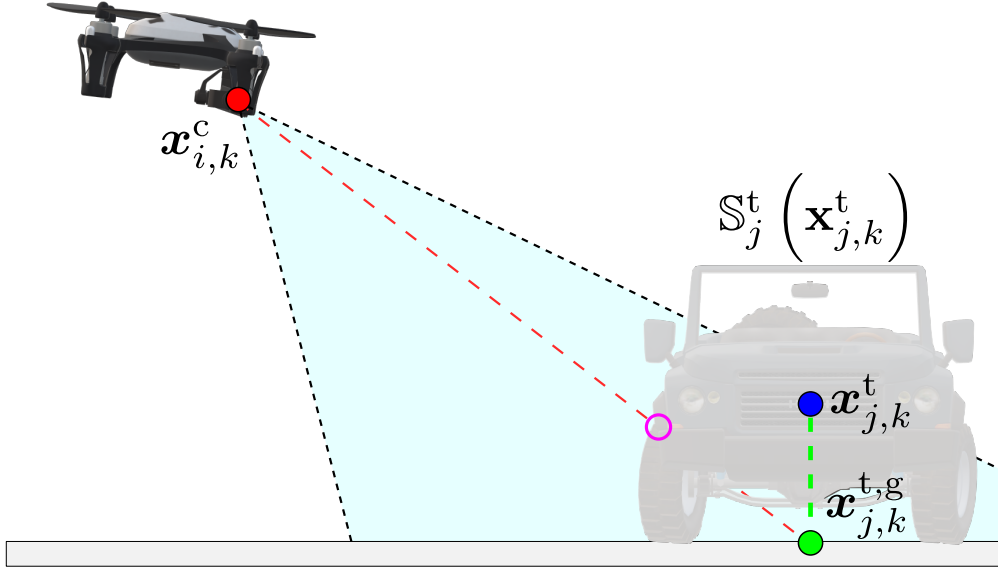


Figure 6. Illustration of (34): The blue and green dots represent respectively $\mathbf{x}_{j,k}^t$ and $\mathbf{x}_{j,k}^{t,g}$; The dashed red line is the line-of-sight $[\mathbf{x}_{i,k}^c, \mathbf{x}_{j,k}^{t,g}]$; The purple dot represents the part of $\mathbb{S}_j^t(\mathbf{x}_j^t)$ seen by the UAV along $[\mathbf{x}_{i,k}^c, \mathbf{x}_{j,k}^{t,g}]$.

C. Assumption on observed targets

Consider some target j such that $\mathbf{x}_j^{t,g} \in \mathbb{F}(\mathbf{x}_i^u)$. We assume that the half-open segment $[\mathbf{x}_i^c, \mathbf{x}_j^{t,g}]$ intersects $\mathbb{S}_j^t(\mathbf{x}_j^t)$, *i.e.*,

$$\mathbf{x}_j^{t,g} \in \mathbb{F}(\mathbf{x}_i^u) \implies [\mathbf{x}_i^c, \mathbf{x}_j^{t,g}] \cap \mathbb{S}_j^t(\mathbf{x}_j^t) \neq \emptyset. \quad (34)$$

Thus, if $\mathbf{x}_j^{t,g}$ belongs to the FoV, then some points on $\mathbb{S}_j^t(\mathbf{x}_j^t)$ will reflect a light ray that will illuminate the CCD array of the camera (in absence of obstacles), see Figure 6. Consequently, if $\mathbf{x}_j^{t,g} \in \mathbb{F}(\mathbf{x}_i^u)$, then there exists a pixel (n_r, n_c) such that $\mathbf{p}_c(\mathbf{x}_i^u, \mathbf{x}_j^{t,g}) \in (n_r, n_c)$. Then according to (34) and (29), $(n_r, n_c) \notin \mathcal{Y}_i^g$.

The assumption (34) is instrumental in the exploration process to characterize parts of \mathbb{X}_g that cannot contain any target location. The validity of this assumption depends on the camera orientation and on the characteristics of the shape $\mathbb{S}_j^t(\mathbf{x}_j^t)$. It is reasonable for many targets such as cars, trucks, provided that they are observed from a location sufficiently above the target, with a camera oriented towards the ground.

V. EXPLOITING CVS INFORMATION FOR SET-MEMBERSHIP ESTIMATION

Section V-A presents an approach to estimate the location of a target j identified at time t_k by the CVS of UAV i . Then, Section V-B describes how the CVS information can be used to characterize a part of \mathbb{X}_g clear of any target. Section V-C presents the characterization of areas occluded by obstacles. In the remainder of this section, the time index k is again omitted to lighten notations.

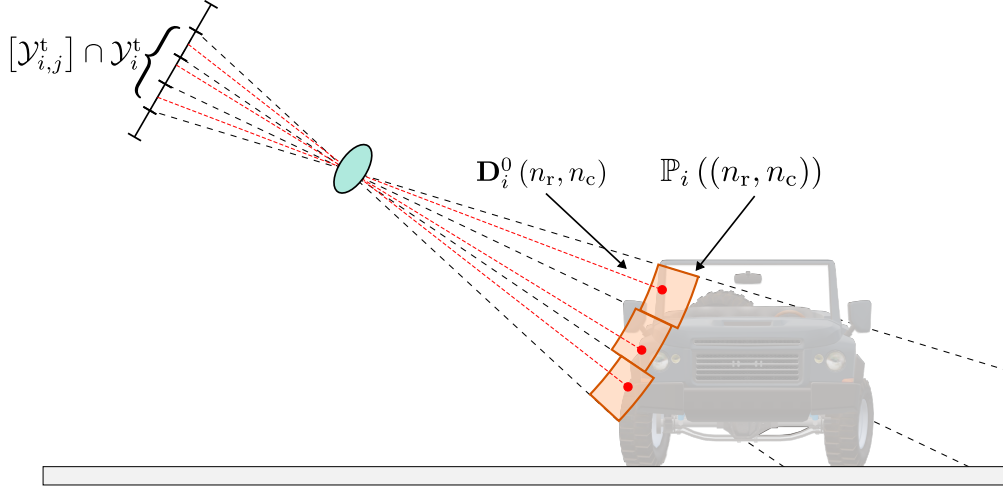


Figure 7. Sets $\mathbb{P}_i((n_r, n_c))$ (in orange) for different $(n_r, n_c) \in [\mathcal{Y}_{i,j}^t]$ and for a target detected and identified by UAV i

A. Estimation of the location of a target

Consider a target j such that $j \in \mathcal{D}_i^t$ with unknown location $\mathbf{x}_j^{t,g}$. UAV i has access to the bounding box $[\mathcal{Y}_{i,j}^t]$, the list of pixel indexes \mathcal{Y}_i^t labeled as Target, and the depth map \mathbf{D}_i . From these measurements related to target j , UAV i has to evaluate a set $\mathbb{X}_{i,j}^{t,m}$ such that $\mathbf{x}_j^{t,g} \in \mathbb{X}_{i,j}^{t,m}$.

For that purpose, a subset of \mathbb{X}_0 with a non-empty intersection with $\mathbb{S}_j^t(\mathbf{x}_j^t)$ is first characterized. For each pixel $(n_r, n_c) \in \mathbf{I}_i$, consider the set

$$\begin{aligned} \mathbb{P}_i((n_r, n_c)) &= \{\mathbf{x} \in \mathbb{F}(\mathbf{x}_i^u) \cap \mathbb{X}_0 \mid \exists \mathbf{v} \in \mathcal{V}_i(n_r, n_c), \\ &\quad d_{\mathbf{v}}(\mathbf{x}_i^c, \{\mathbf{x}\}) \in [\mathbf{D}_i](n_r, n_c)\} \end{aligned} \quad (35)$$

of all points in $\mathbb{F}(\mathbf{x}_i^u) \cap \mathbb{X}_0$ that may have contributed to the illumination of (n_r, n_c) while being at a distance from UAV i consistent with $\mathbf{D}_i(n_r, n_c)$, see Figure 7.

According to (32), $\mathcal{Y}_{i,j}^t \neq \emptyset$. Moreover, from (33), one has $\mathcal{Y}_{i,j}^t \subset [\mathcal{Y}_{i,j}^t]$. Nevertheless, as indicated in Section IV-B3, only the set of pixels \mathcal{Y}_i^t such that $\mathcal{Y}_{i,j}^t \subset \mathcal{Y}_i^t$ is available. Proposition 1 states that there exists at least one pixel (n_r, n_c) in $[\mathcal{Y}_{i,j}^t] \cap \mathcal{Y}_i^t$ for which the set $\mathbb{P}_i((n_r, n_c))$ intersects $\mathbb{S}_j^t(\mathbf{x}_j^t)$.

Proposition 1. *If $j \in \mathcal{D}_i^t$, then $\exists (n_r, n_c) \in [\mathcal{Y}_{i,j}^t] \cap \mathcal{Y}_i^t$ such that $\mathbb{P}_i((n_r, n_c)) \cap \mathbb{S}_j^t(\mathbf{x}_j^t) \neq \emptyset$.*

Proof: If $j \in \mathcal{D}_i^t$, then $\mathcal{Y}_{i,j}^t \neq \emptyset$ and $\mathcal{Y}_{i,j}^t \subset [\mathcal{Y}_{i,j}^t]$. Combining (32), (33), and (30), $\exists (n_r, n_c) \in [\mathcal{Y}_{i,j}^t] \cap \mathcal{Y}_i^t$ such that for all $\mathbf{v} \in \mathcal{V}_i(n_r, n_c)$, $\rho(\mathbf{x}_i^u, \mathbf{v}) = d_{\mathbf{v}}(\mathbf{x}_i^c, \mathbb{S}_j^t(\mathbf{x}_j^t))$. Therefore, $\exists \mathbf{v} \in \mathcal{V}_i(n_r, n_c)$ and $\exists \mathbf{x} \in \mathbb{S}_j^t(\mathbf{x}_j^t)$ such that $d_{\mathbf{v}}(\mathbf{x}_i^c, \{\mathbf{x}\}) = \mathbf{D}_i^0(n_r, n_c)$. As $(n_r, n_c) \in \mathcal{Y}_i^t \subset \mathcal{Y}_i$, according to (28), $\mathbf{D}_i(n_r, n_c) / (1 + \underline{w}) \leq d_{\max}$ and $d_{\mathbf{v}}(\mathbf{x}_i^c, \{\mathbf{x}\}) \leq d_{\max}$. Then $\mathbf{x} \in \mathbb{F}(\mathbf{x}_i^u)$. Finally, from (35), we have $\mathbf{x} \in \mathbb{P}_i((n_r, n_c))$. So $\mathbb{P}_i((n_r, n_c)) \cap \mathbb{S}_j^t(\mathbf{x}_j^t) \neq \emptyset$. ■

According to Proposition 1, a pixel (n_r, n_c) such that $\mathbb{P}_i((n_r, n_c)) \cap \mathbb{S}_j^t(\mathbf{x}_j^t) \neq \emptyset$ exists, but it is only known to belong to $\mathcal{Y}_i^t \cap [\mathcal{Y}_{i,j}^t]$. To get a set intersecting $\mathbb{S}_j^t(\mathbf{x}_j^t)$, one has then to consider the union of all sets $\mathbb{P}_i((n_r, n_c))$

for the pixels $(n_r, n_c) \in [\mathcal{Y}_{i,j}^t] \cap \mathcal{Y}_i^t$, see Corollary 2, a direct consequence of Proposition 1.

Corollary 2. *If $j \in \mathcal{D}_i^t$, then the set*

$$\mathbb{P}_{i,j}^t = \bigcup_{(n_r, n_c) \in [\mathcal{Y}_{i,j}^t] \cap \mathcal{Y}_i^t} \mathbb{P}_i((n_r, n_c)) \quad (36)$$

is such that $\mathbb{P}_{i,j}^t \cap \mathbb{S}_j^t(\mathbf{x}_j^t) \neq \emptyset$.

Again, $\mathbb{P}_{i,j}^t$ is only known to intersect $\mathbb{S}_j^t(\mathbf{x}_j^t)$. If $\mathbf{x} \in \mathbb{P}_{i,j}^t \cap \mathbb{S}_j^t(\mathbf{x}_j^t)$ would be available, exploiting the fact that $\mathbb{S}_j^t(\mathbf{x}_j^t) \subset \mathbb{C}^t(\mathbf{x}_j^{t,g})$, one would have $\mathbf{x}_j^{t,g} \in \mathbb{D}_g(\mathbf{p}_g(\mathbf{x}), r^t)$, see the proof of Proposition 3, below. The set estimate $\mathbb{X}_{i,j}^{t,m}$ of $\mathbf{x}_j^{t,g}$ introduced in Proposition 3 accounts for the fact that \mathbf{x} is only known to belong to $\mathbb{P}_{i,j}^t$.

Proposition 3. *If $j \in \mathcal{D}_i^t$, then the set estimate*

$$\mathbb{X}_{i,j}^{t,m} = \bigcup_{\mathbf{x} \in \mathbf{p}_g(\mathbb{P}_{i,j}^t)} \mathbb{D}_g(\mathbf{x}, r^t) \quad (37)$$

is such that $\mathbf{x}_j^{t,g} \in \mathbb{X}_{i,j}^{t,m}$.

Proof: As $j \in \mathcal{D}_i^t$, from Corollary 2, $\mathbb{P}_{i,j}^t \cap \mathbb{S}_j^t(\mathbf{x}_j^t) \neq \emptyset$. Consequently, $\mathbf{p}_g(\mathbb{P}_{i,j}^t) \cap \mathbf{p}_g(\mathbb{S}_j^t(\mathbf{x}_j^t)) \neq \emptyset$ and there exists $\mathbf{x} \in \mathbf{p}_g(\mathbb{P}_{i,j}^t) \cap \mathbf{p}_g(\mathbb{S}_j^t(\mathbf{x}_j^t)) \subset \mathbf{p}_g(\mathbb{S}_j^t(\mathbf{x}_j^t))$. Since $\mathbb{S}_j^t(\mathbf{x}_j^t) \subset \mathbb{C}^t(\mathbf{x}_j^{t,g})$, $\mathbf{p}_g(\mathbb{S}_j^t(\mathbf{x}_j^t)) \subset \mathbf{p}_g(\mathbb{C}^t(\mathbf{x}_j^{t,g}))$ and $\mathbf{x} \in \mathbf{p}_g(\mathbb{C}^t(\mathbf{x}_j^{t,g}))$. As $\mathbf{p}_g(\mathbb{C}^t(\mathbf{x}_j^{t,g})) = \mathbb{D}_g(\mathbf{x}_j^{t,g}, r^t)$, one has $\|\mathbf{x} - \mathbf{x}_j^{t,g}\| \leq r^t$ and $\mathbf{x}_j^{t,g} \in \mathbb{D}_g(\mathbf{x}, r^t)$. Consequently, $\mathbf{x}_j^{t,g} \in \bigcup_{\mathbf{x} \in \mathbf{p}_g(\mathbb{P}_{i,j}^t)} \mathbb{D}_g(\mathbf{x}, r^t)$. ■

Determining $\mathbf{x} \in \mathbf{p}_g(\mathbb{P}_{i,j}^t) \cap \mathbf{p}_g(\mathbb{S}_j^t(\mathbf{x}_j^t))$ without knowing $\mathbb{S}_j^t(\mathbf{x}_j^t)$ is difficult. This is why the estimate $\mathbb{X}_{i,j}^{t,m}$ is defined considering all $\mathbf{x} \in \mathbf{p}_g(\mathbb{P}_{i,j}^t)$ as $\mathbf{p}_g(\mathbb{P}_{i,j}^t) \cap \mathbf{p}_g(\mathbb{S}_j^t(\mathbf{x}_j^t)) \subset \mathbf{p}_g(\mathbb{P}_{i,j}^t)$. In practice, the estimate $\mathbb{X}_{i,j}^{t,m}$ is evaluated as

$$\mathbb{X}_{i,j}^{t,m} = \mathbb{X}_g \cap (\mathbf{p}_g(\mathbb{P}_{i,j}^t) \oplus \mathbb{D}_g(\mathbf{0}, r^t)), \quad (38)$$

which, compared to (37), only involves the Minkovski sum of the disc $\mathbb{D}_g(\mathbf{0}, r^t)$ and the projection of $\mathbb{P}_{i,j}^t$ on \mathbb{X}_g , see Figure 8. Appendix A describes the practical evaluation of $\mathbb{X}_{i,j}^{t,m}$.

B. Estimation of the space free of target

In what follows, using \mathbf{L}_i and \mathbf{D}_i , one characterizes a subset of \mathbb{X}_g which contains no target location. For that purpose, pixels labeled as Ground and as Obstacles are used respectively in Sections V-B1 and V-B2.

1) *Using pixels labeled as Ground:* For each pixel (n_r, n_c) , the set

$$\mathbb{P}_i^g((n_r, n_c)) = \{\mathbf{x} \in \mathbb{F}(\mathbf{x}_i^u) \cap \mathbb{X}_g \mid \mathbf{p}_c(\mathbf{x}_i^u, \mathbf{x}) \in (n_r, n_c)\} \quad (39)$$

contains all points in $\mathbb{F}(\mathbf{x}_i^u) \cap \mathbb{X}_g$, the intersection of the FoV with the ground, which image in the CCD array belongs to (n_r, n_c) . According to (29), pixels in \mathcal{Y}_i^g , i.e., labeled as Ground, are such that only points in \mathbb{X}_g have contributed to their illumination. Consequently, the set

$$\mathbb{P}_i^g(\mathcal{Y}_i^g) = \{\mathbf{x} \in \mathbb{F}(\mathbf{x}_i^u) \cap \mathbb{X}_g \mid \mathbf{p}_c(\mathbf{x}_i^u, \mathbf{x}) \in \mathcal{Y}_i^g\} \quad (40)$$

of points of \mathbb{X}_g which image in the CCD array belongs to a pixel classified as ground, cannot contain the location of a target, see Proposition 4.

Proof: First, if $\mathbf{x}_j^{\mathbf{t}_g} \notin \mathbb{F}(\mathbf{x}_i^{\mathbf{u}})$, then $\mathbf{x}_j^{\mathbf{t}_g} \notin \mathbb{P}_i^g(\mathcal{Y}_i^g)$ by definition of $\mathbb{P}_i^g(\mathcal{Y}_i^g)$. Assume now that $\mathbf{x}_j^{\mathbf{t}_g} \in \mathbb{F}(\mathbf{x}_i^{\mathbf{u}})$. According to (23), there exists $(n_r, n_c) \in \mathcal{N}^1$ such that $\mathbf{p}_c(\mathbf{x}_i^{\mathbf{u}}, \mathbf{x}_j^{\mathbf{t}_g}) \in (n_r, n_c)$. Moreover, according to (34), there exists a half-open segment $[\mathbf{x}_i^c, \mathbf{x}_j^{\mathbf{t}_g}[$ such that $[\mathbf{x}_i^c, \mathbf{x}_j^{\mathbf{t}_g}[\cap \mathcal{S}_j^{\mathbf{t}}(\mathbf{x}_j^{\mathbf{t}}) \neq \emptyset$ while $[\mathbf{x}_i^c, \mathbf{x}_j^{\mathbf{t}_g}[\cap \mathbb{X}_g = \emptyset$. Consider the unit vector $\mathbf{v} \in \mathcal{V}_i(n_r, n_c)$ such that \mathbf{v} is colinear with $[\mathbf{x}_i^c, \mathbf{x}_j^{\mathbf{t}_g}[$. Therefore, $\rho(\mathbf{x}_i^{\mathbf{u}}, \mathbf{v}) \neq d_{\mathbf{v}}(\mathbf{x}_i^c, \mathbb{X}_g)$ and, according to (29), $\mathbf{p}_c(\mathbf{x}_i^{\mathbf{u}}, \mathbf{x}_j^{\mathbf{t}_g}) \notin \mathcal{Y}_i^g$. Consequently, from (40), $\mathbf{x}_j^{\mathbf{t}_g} \notin \mathbb{P}_i^g(\mathcal{Y}_i^g)$. \blacksquare

2) *Using pixels labeled as Obstacle:* UAV i is able to characterize an inner-approximation $\underline{\mathbb{X}}_i^o \subset \mathbb{X}_g$ of the r^s -ground neighborhood of $\bigcup_{m \in \mathcal{N}^o} p_g(\mathbb{S}_m^o)$, the union of the projection on the ground of the shape of all obstacles. According to (9), the distance between a target location and the projection on the ground of any obstacle is at least r^s . Consequently, the set $\underline{\mathbb{X}}_i^o$ does not contain any target location.

Proof: If $(n_r, n_c) \in \mathcal{Y}_i^0$, then, according to (31), for all $\mathbf{v} \in \mathcal{V}_i(n_r, n_c)$, there exists $m \in \mathcal{N}^0$ such that $\rho(\mathbf{x}_i^u, \mathbf{v}) = d_v(\mathbf{x}_i^c, \mathbb{S}_m^0)$. Therefore, there exists $\mathbf{v} \in \mathcal{V}_i(n_r, n_c)$ and there exists $\mathbf{x} \in \mathbb{S}_m^0$ such that $d_v(\mathbf{x}_i^c, \{\mathbf{x}\}) = \mathbf{D}_i^0(n_r, n_c)$. Consequently, from (35), $\mathbf{x} \in \mathbb{P}_i((n_r, n_c))$. So there exists $m \in \mathcal{N}^0$ such that $\mathbb{P}_i((n_r, n_c)) \cap \mathbb{S}_m^0 \neq \emptyset$.

If some $\mathbf{x} \in \mathbb{P}_i((n_r, n_c)) \cap \mathbb{S}_m^o$ would be known, then, according to (9), one would be able to prove that there is no target location in $\mathbb{N}_g(\{\mathbf{x}\}, r^s)$, the r^s -ground neighborhood of \mathbf{x} . As $\mathbb{P}_i((n_r, n_c)) \cap \mathbb{S}_m^o \subset \mathbb{P}_i((n_r, n_c))$, one considers the set

$$\mathbb{S}^o((n_r, n_c), r^s) = \bigcap_{\mathbf{x} \in \mathbb{P}_i((n_r, n_c))} \mathbb{N}_g(\{\mathbf{x}\}, r^s). \quad (41)$$

defined as the intersections of all r^s -ground neighborhood of $\mathbf{x} \in \mathbb{P}_i((n_r, n_c))$. The following proposition states that $\mathbb{S}^o((n_r, n_c), r^s)$ is an inner-approximation of the r^s -ground neighborhood of an obstacle.

Proposition 6. *If $(n_r, n_c) \in \mathcal{Y}_i^o$, then there exists $m \in \mathcal{N}^o$, such that*

$$\mathbb{S}^o((n_r, n_c), r^s) \subset \mathbb{N}_g(\mathbb{S}_m^o, r^s). \quad (42)$$

Proof: If $(n_r, n_c) \in \mathcal{Y}_i^o$, then, according to Proposition 5, there exists $m \in \mathcal{N}^o$ such that $\mathbb{P}_i((n_r, n_c)) \cap \mathbb{S}_m^o \neq \emptyset$. As $\mathbb{P}_i((n_r, n_c)) \cap \mathbb{S}_m^o \subset \mathbb{P}_i((n_r, n_c))$, one has

$$\bigcap_{\mathbf{x} \in \mathbb{P}_i((n_r, n_c))} \mathbb{N}_g(\{\mathbf{x}\}, r^s) \subset \bigcap_{\mathbf{x} \in \mathbb{P}_i((n_r, n_c)) \cap \mathbb{S}_m^o} \mathbb{N}_g(\{\mathbf{x}\}, r^s). \quad (43)$$

Moreover, as $\mathbb{P}_i((n_r, n_c)) \cap \mathbb{S}_m^o \subset \mathbb{S}_m^o$,

$$\bigcap_{\mathbf{x} \in \mathbb{P}_i((n_r, n_c)) \cap \mathbb{S}_m^o} \mathbb{N}_g(\{\mathbf{x}\}, r^s) \subset \bigcup_{\mathbf{x} \in \mathbb{S}_m^o} \mathbb{N}_g(\{\mathbf{x}\}, r^s) = \mathbb{N}_g(\mathbb{S}_m^o, r^s). \quad (44)$$

Combining the two previous inclusions, one gets (42). ■

An inner-approximation of the r^s -ground neighborhood of all the obstacles located within the FoV of UAV i can then be obtained by characterizing the union of the sets $\mathbb{S}^o((n_r, n_c), r^s)$ for all pixels $(n_r, n_c) \in \mathcal{Y}_i^o$. Then using Proposition 7, UAV i is able to evaluate a set $\underline{\mathbb{X}}_i^o$ which cannot contain any target location.

Proposition 7. *If $\mathcal{Y}_i^o \neq \emptyset$, then the set*

$$\underline{\mathbb{X}}_i^o = \bigcup_{(n_r, n_c) \in \mathcal{Y}_i^o} \mathbb{S}^o((n_r, n_c), r^s) \quad (45)$$

is such that $\mathbf{x}_j^{t,g} \notin \underline{\mathbb{X}}_i^o$, for all $j \in \mathcal{N}^t$.

Proof: Using Proposition 6, for each $(n_r, n_c) \in \mathcal{Y}_i^o$, there exists $m \in \mathcal{N}^o$ such that $\mathbb{S}^o((n_r, n_c), r^s) \subset \mathbb{N}_g(\mathbb{S}_m^o, r^s)$. Consequently,

$$\bigcup_{(n_r, n_c) \in \mathcal{Y}_i^o} \mathbb{S}^o((n_r, n_c), r^s) \subset \bigcup_{m \in \mathcal{N}^o} \mathbb{N}_g(\mathbb{S}_m^o, r^s). \quad (46)$$

Consequently $\underline{\mathbb{X}}_i^o \subset \bigcup_{m \in \mathcal{N}^o} \mathbb{N}_g(\mathbb{S}_m^o, r^s)$. According to Assumption 9, we have

$$\begin{aligned} \forall j \in \mathcal{N}^t, \forall m \in \mathcal{N}^o, \mathbf{x}_j^{t,g} &\notin \mathbb{N}_g(\mathbb{S}_m^o, r^s) \\ \Leftrightarrow \forall j \in \mathcal{N}^t, \mathbf{x}_j^{t,g} &\notin \bigcup_{m \in \mathcal{N}^o} \mathbb{N}_g(\mathbb{S}_m^o, r^s) \end{aligned} \quad (47)$$

therefore $\forall j \in \mathcal{N}^t, \mathbf{x}_j^{t,g} \notin \underline{\mathbb{X}}_i^o$. ■

Appendix A describes the practical evaluation of $\underline{\mathbb{X}}_i^o$.

C. Estimation of the hidden area

Some parts of $\mathbb{F}(\mathbf{x}_i^u) \cap \mathbb{X}_g$ cannot be seen by UAV i when they are hidden by an obstacle, a target, or a UAV. The pixels labeled either as Obstacle, Target, or Unknown are used to characterize the hidden parts of $\mathbb{F}(\mathbf{x}_i^u) \cap \mathbb{X}_g$, denoted as

$$\mathbb{H}_i^g = \mathbb{P}_i^g(\mathcal{Y}_i^o \cup \mathcal{Y}_i^t \cup \mathcal{Y}_i^n) \quad (48)$$

$$= \bigcup_{(n_r, n_c) \in \mathcal{Y}_i^o \cup \mathcal{Y}_i^t \cup \mathcal{Y}_i^n} \mathbb{P}_i^g((n_r, n_c)). \quad (49)$$

\mathbb{H}_i^g represent the part of the ground that is hidden by obstacles or targets, or for which no reliable enough information is available. \mathbb{H}_i^g will be useful in the UAV exploration process.

Appendix B describes the practical evaluation of \mathbb{H}_i^g .

VI. ESTIMATION ALGORITHM

This section describes the way a distributed set-membership target location estimator exploits the information provided by the CVS. It is adapted from [13]. Only the parts related to the exploitation of the CVS are detailed here. The set estimates are initialized at time t_0 as $\mathcal{L}_{i,0}^t = \emptyset$, $\mathcal{X}_{i,0}^t = \emptyset$, $\bar{\mathbb{X}}_{i,0}^t = \mathbb{X}_g$, and $\mathbb{X}_{i,0}^o = \emptyset$.

A. Prediction step

At time t_k , the predicted set $\mathbb{X}_{i,j,k|k-1}^t$ of possible future locations of identified target $j \in \mathcal{L}_{i,k}^t$ is evaluated using the set of previous locations $\mathbb{X}_{i,j,k-1}^t$, the target dynamics (2), and the known bounds of its control input

$$\mathbb{X}_{i,j,k|k-1}^t = \mathbf{f}^t(\mathbb{X}_{i,j,k-1}^t, [\mathbf{v}^t]) \cap \mathbb{X}_g. \quad (50)$$

In the same way, the predicted set $\bar{\mathbb{X}}_{i,k|k-1}^t$ for all possible locations of targets still to be identified is

$$\bar{\mathbb{X}}_{i,k|k-1}^t = \mathbf{f}^t(\bar{\mathbb{X}}_{i,k-1}^t, [\mathbf{v}^t]) \cap \mathbb{X}_g. \quad (51)$$

Obstacles being statics, the predicted set $\mathbb{X}_{i,k|k-1}^o$ is

$$\mathbb{X}_{i,k|k-1}^o = \mathbb{X}_{i,k-1}^o. \quad (52)$$

B. Updates from measurements

The CVS of UAV i provides $\mathbf{I}_{i,k}$, $\mathbf{L}_{i,k}$, $\mathbf{D}_{i,k}$, $\mathcal{D}_{i,k}^t$, and $\mathcal{B}_{i,k}^t$. Then $\mathcal{Y}_{i,k}^t$, $\mathcal{Y}_{i,k}^g$, and $\mathcal{Y}_{i,k}^o$ are directly obtained from $\mathbf{L}_{i,k}$ and $\mathbf{D}_{i,k}$, see Section IV-B2. Moreover, $\mathbb{X}_{i,j,k}^{t,m}$ is deduced from $\mathcal{Y}_{i,k}^t$ and $[\mathcal{Y}_{i,j,k}^t]$ for all $j \in \mathcal{D}_{i,k}^t$ using (36) and (38).

First, using the set of newly identified targets $\mathcal{D}_{i,k}^t$, the list of all identified targets becomes $\mathcal{L}_{i,k|k}^t = \mathcal{L}_{i,k-1}^t \cup \mathcal{D}_{i,k}^t$.

According to Sections V-B1 and V-B2, the set $\mathbb{P}_{i,k}^g(\mathcal{Y}_{i,k}^g) \cup \mathbb{X}_{i,k|k}^o$ is proved to be free of target. Therefore, the set $\bar{\mathbb{X}}_{i,k|k-1}^t$ is updated as

$$\bar{\mathbb{X}}_{i,k|k}^t = \bar{\mathbb{X}}_{i,k|k-1}^t \setminus \left(\mathbb{P}_{i,k}^g(\mathcal{Y}_{i,k}^g) \cup \mathbb{X}_{i,k|k}^o \right). \quad (53)$$

Moreover, for each previously identified target $j \in \mathcal{L}_{i,k-1}^t \setminus \mathcal{D}_{i,k}^t$ which is not identified at time t_k , $\mathbb{X}_{i,j,k|k-1}^t$ is updated as

$$\mathbb{X}_{i,j,k|k}^t = \mathbb{X}_{i,j,k|k-1}^t \setminus \left(\mathbb{P}_{i,k}^g \left(\mathcal{Y}_{i,k}^g \right) \cup \mathbb{X}_{i,k|k}^o \right). \quad (54)$$

If target j is identified at time t_k , i.e., $j \in \mathcal{D}_{i,k}^t$, then $\mathbf{x}_{j,k}^{t,g} \in \mathbb{X}_{i,j,k}^{t,m}$, see Section V-A. Moreover, if $j \in \mathcal{L}_{i,k-1}^t$, one has also $\mathbf{x}_{j,k}^{t,g} \in \mathbb{X}_{i,j,k|k-1}^t$ else $\mathbf{x}_{j,k}^{t,g} \in \bar{\mathbb{X}}_{i,k|k-1}^t$. Therefore, for each target $j \in \mathcal{D}_{i,k}^t$, one has, if $j \in \mathcal{L}_{i,k-1}^t$

$$\mathbb{X}_{i,j,k|k}^t = \left(\mathbb{X}_{i,j,k|k-1}^t \cap \mathbb{X}_{i,j,k}^{t,m} \right) \setminus \left(\mathbb{P}_{i,k}^g \left(\mathcal{Y}_{i,k}^g \right) \cup \mathbb{X}_{i,k|k}^o \right), \quad (55)$$

and if $j \notin \mathcal{L}_{i,k-1}^t$

$$\mathbb{X}_{i,j,k|k}^t = \left(\bar{\mathbb{X}}_{i,k|k-1}^t \cap \mathbb{X}_{i,j,k}^{t,m} \right) \setminus \left(\mathbb{P}_{i,k}^g \left(\mathcal{Y}_{i,k}^g \right) \cup \mathbb{X}_{i,k|k}^o \right).$$

Finally, the r_s -neighborhoods of all obstacles is updated as

$$\mathbb{X}_{i,k|k}^o = \mathbb{X}_{i,k-1}^o \cup \underline{\mathbb{X}}_{i,k}^o, \quad (56)$$

see Section V-B2.

C. Update after communication with neighbors

Each UAV ℓ , once it has taken into account its own measurements, broadcasts the list of identified targets $\mathcal{L}_{\ell,k|k}^t$, the r_s -neighborhoods of obstacles $\mathbb{X}_{\ell,k|k}^o$, the set estimates $\mathbb{X}_{\ell,j,k|k}^t$, $j \in \mathcal{L}_{\ell,k|k}^t$ and the set of possible locations of targets still to be identified $\bar{\mathbb{X}}_{\ell,k|k}^t$.

Accounting for the information received from its neighbors, UAV i updates the list of identified targets as $\mathcal{L}_{i,k}^t = \bigcup_{\ell \in \mathcal{N}_{i,k}} \mathcal{L}_{\ell,k|k}^t$, the r_s -neighborhoods of obstacles $\mathbb{X}_{i,k}^o = \bigcup_{\ell \in \mathcal{N}_{i,k}} \mathbb{X}_{\ell,k|k}^o$, and the set of possible locations of targets still to be identified $\bar{\mathbb{X}}_{i,k}^t = \bigcap_{\ell \in \mathcal{N}_{i,k}} \bar{\mathbb{X}}_{\ell,k|k}^t$. Then, if $j \in \mathcal{L}_{i,k}^t$, one has

$$\mathbb{X}_{i,j,k}^t = \bigcap_{\substack{\ell \in \mathcal{N}_{i,k} \\ \text{st } j \in \mathcal{L}_{\ell,k|k}^t}} \mathbb{X}_{\ell,j,k|k}^t \cap \bigcap_{\substack{\ell \in \mathcal{N}_{i,k} \\ \text{st } j \notin \mathcal{L}_{\ell,k|k}^t}} \bar{\mathbb{X}}_{\ell,k|k}^t. \quad (57)$$

to account (i) for the estimate $\mathbb{X}_{\ell,j,k|k}^t$ of the location of target j made by the neighbors of UAV i which have already identified target j and (ii) for the fact that $\mathbf{x}_{j,k}^t \in \bar{\mathbb{X}}_{\ell,k|k}^t$ for all neighbors of UAV i which have not yet identified target j .

VII. EVALUATION OF UAV TRAJECTORIES

The trajectory of UAV i is designed so as to minimize the estimation uncertainty of target locations (11). For that purpose, a distributed MPC approach [60] is used, based on that presented in [13]. At time t_k , the trajectory of UAV i is determined over a prediction horizon h by evaluating a sequence of control inputs $\mathbf{u}_{i,k:h}^p = (\mathbf{u}_{i,k}^p, \dots, \mathbf{u}_{i,k+h-1}^p) \in \mathbb{U} \times \dots \times \mathbb{U}$, from which a sequence of states $\mathbf{x}_{i,k:h}^{u,p} = (\mathbf{x}_{i,k+1|k}^{u,p}, \dots, \mathbf{x}_{i,k+h|k}^{u,p})$ is deduced using (10), so as to minimize the criterion

$$J_0(\mathbf{u}_{i,k:h}^p) = \Phi \left(\mathcal{X}_{i,k+h|k}^{t,p}, \bar{\mathbb{X}}_{i,k+h|k}^{t,p} \right). \quad (58)$$

The sequence of predicted states $\mathbf{x}_{i,k:h}^{u,p}$ is then fed as a desired state target to the low-level controller for UAV i , responsible of evaluating high-frequency control inputs. In (58), $\mathcal{X}_{i,k+h|k}^{t,p}$ is the list of predicted estimates of the

target locations $\mathbb{X}_{i,j,k+h|k}^{\text{t,P}}$ for all $j \in \mathcal{L}_{i,k}^{\text{t}}$, and $\bar{\mathbb{X}}_{i,k+h|k}^{\text{t,P}}$ is the predicted set of possible locations of targets still to be identified, both evaluated at time t_{k+h} using the information available at time t_k . See [13] for more details.

In some cases, $J_0(\mathbf{u}_{i,k:h}^{\text{P}})$ remains constant whatever $\mathbf{u}_{i,k:h}^{\text{P}} \in \mathbb{U}^h$. This may occur once large parts of the environment have been explored. A second criterion is introduced

$$J_1(\mathbf{u}_{i,k:h}^{\text{P}}) = d\left(c\left(\mathbb{F}\left(\mathbf{x}_{i,k+h|k}^{\text{u,P}}\right) \cap \mathbb{X}_{\text{g}}\right), \left(\bar{\mathbb{X}}_{i,k+h|k}^{\text{t,P}} \cup \bigcup_{j \in \mathcal{L}_{i,k}^{\text{t}}} \mathbb{X}_{i,j,k+h|k}^{\text{t,P}}\right) \setminus \mathbb{H}_{i,k}^{\text{g}}\right), \quad (59)$$

where $c(\mathbb{X})$ is the barycenter of the set \mathbb{X} . The idea is to drive the FoV of UAV i to the closest predicted set estimate related to an identified target or to the part of the search area where targets may have still to be identified. To account for possible occlusions by obstacles, we assume that the part $\mathbb{H}_{i,k}^{\text{g}}$ of the ground hidden at time t_k does not evolve during the h next time steps.

The resulting criterion combining (58) and (59) is

$$J(\mathbf{u}_{i,k:h}^{\text{P}}) = J_0(\mathbf{u}_{i,k:h}^{\text{P}}) + \lambda J_1(\mathbf{u}_{i,k:h}^{\text{P}}). \quad (60)$$

where λ trades off the direct reduction of the size of the set estimates via $J_0(\mathbf{u}_{i,k:h}^{\text{P}})$ and future reductions via $J_1(\mathbf{u}_{i,k:h}^{\text{P}})$.

Compared to [13], $J_1(\mathbf{u}_{i,k:h}^{\text{P}})$ and the characterization of $\mathcal{X}_{i,k+h|k}^{\text{t,P}}$ and $\bar{\mathbb{X}}_{i,k+h|k}^{\text{t,P}}$ take into account the occluded part of the ground $\mathbb{H}_{i,k}^{\text{g}}$ that UAV i has not observed at time t_k . The aim is to drive the UAVs toward areas which are less likely to be occluded by obstacles.

VIII. SIMULATIONS

Simulations results have been obtained using Webots [61] to generate UAV and target displacements as well as the measurements collected by the UAVs. The set estimators and trajectory design algorithms are implemented on Matlab.

A. Simulation conditions

The RoI is a simplified urban environment with different types of buildings with a height less than 50 m, see Figure 9. One has $\mathbb{X}_0 = [-250 \text{ m}, 250 \text{ m}] \times [-250 \text{ m}, 250 \text{ m}] \times \mathbb{R}^+$. The ground area occupied by building represents 5 % of the total area of \mathbb{X}_{g} . The RoI contains $N^{\text{t}} = 8$ targets (cars of the same shape).

Each car has the following dimensions $4.6 \text{ m} \times 1.8 \text{ m} \times 1.5 \text{ m}$, and can be included in a cylinder \mathbb{C}^{t} of radius $r^{\text{t}} = 2.5 \text{ m}$ and height $h^{\text{t}} = 2 \text{ m}$. The safety distance is taken as $r_{\text{s}}^{\text{to}} = 3 \text{ m}$. The state $\mathbf{x}_{j,k}^{\text{t}} = (x_{j,1,k}^{\text{t}}, x_{j,2,k}^{\text{t}}, x_{j,3,k}^{\text{t}})$ of target $j \in \mathcal{N}^{\text{t}}$ consists of the coordinates $(x_{j,1,k}^{\text{t}}, x_{j,2,k}^{\text{t}})$ of the projection on \mathbb{X}_{g} of its center of mass, and of its heading angle $x_{j,3,k}^{\text{t}}$. Its dynamic (2) is

$$\begin{pmatrix} x_{j,1,k+1}^{\text{t}} \\ x_{j,2,k+1}^{\text{t}} \\ x_{j,3,k+1}^{\text{t}} \end{pmatrix} = \begin{pmatrix} x_{j,1,k}^{\text{t}} + Tv_{j,1}^{\text{t}} \cos(x_{j,3,k}^{\text{t}}) \\ x_{j,2,k}^{\text{t}} + Tv_{j,1}^{\text{t}} \sin(x_{j,3,k}^{\text{t}}) \\ x_{j,3,k}^{\text{t}} + Tv_{j,2,k}^{\text{t}} \end{pmatrix}, \quad (61)$$

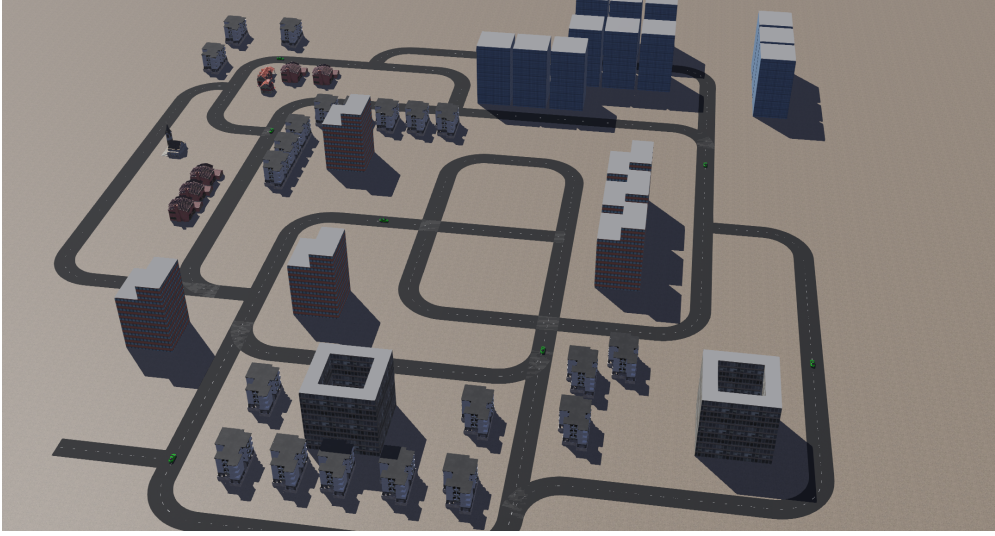


Figure 9. Simulated urban environment in Webots

where $v_{j,1}^t$ is the constant target speed and $v_{j,2,k}^t$ is the target turn rate. At the start of the simulation, for each target $j \in \mathcal{N}^t$, $v_{j,1}^t$ is randomly chosen in the interval $[0, v_{\max}]$. Here, only $v_{\max} = 1$ m/s is known to the UAVs. At each time instant, $v_{j,2,k}^t$ is constrained to maintain the car on the roads. The UAVs do not exploit any knowledge related to the roads during the search.

A fleet of 4 identical quadcopters is considered (the DJI Mavic2Pro model in Webots). These UAVs are assumed to be equipped with a camera of resolution $N_r \times N_c = 360 \times 480$ pixels, aperture angle of $\pi/4$ rad, and orientation in the UAV body frame of $\theta = \pi/6$ rad. A depth map is provided by the *range finder* of Webots with the same resolution as the camera. Its maximal measurement range is set to $d_{\max} = 300$ m and the bounds of the noise w in (26) are $[w, \bar{w}] = [-1\%, 1\%]$. For example, if the distance $\mathbf{D}_i^0(n_r, n_c)$ to an object is 200 m, then the depth-map measurement $\mathbf{D}_i(n_r, n_c)$ is obtained by randomly selecting $w \in [w, \bar{w}] = [-1\%, 1\%]$, to get, for example, $\mathbf{D}_i(n_r, n_c) = 201$ m. Then, using (27), one gets $[\mathbf{D}_i](n_r, n_c) = [199.01 \text{ m}, 203.03 \text{ m}]$. Figure 10 shows an example of CVS information provided to each UAV.

CVS provides information with a period $T = 0.5$ s. The set estimates are updated with the same period using the algorithms presented in Sections V and VI. The trajectories of UAVs are updated with a period of $T^{\text{MPC}} = 3$ s due to the flight time constants of the quadcopters. This choice ensures that each UAV reaches the desired target state designed by the MPC approach. Furthermore, no restriction is considered on the communication range between UAVs.

All UAVs are launched from the same location outside the RoI. For the UAV trajectory design in the MPC approach, a simple dynamic model with constant altitude and speed v^u , as well as null roll and pitch angles is considered

$$\begin{pmatrix} x_{i,1,k+1}^u \\ x_{i,2,k+1}^u \\ x_{i,3,k+1}^u \\ x_{i,4,k+1}^u \end{pmatrix} = \begin{pmatrix} x_{i,1,k}^u + Tv^u \cos(x_{i,4,k}^u + u_{i,k}) \\ x_{i,2,k}^u + Tv^u \sin(x_{i,4,k}^u + u_{i,k}) \\ x_{i,3,k+1}^u \\ x_{i,4,k}^u + u_{i,k} \end{pmatrix}. \quad (62)$$

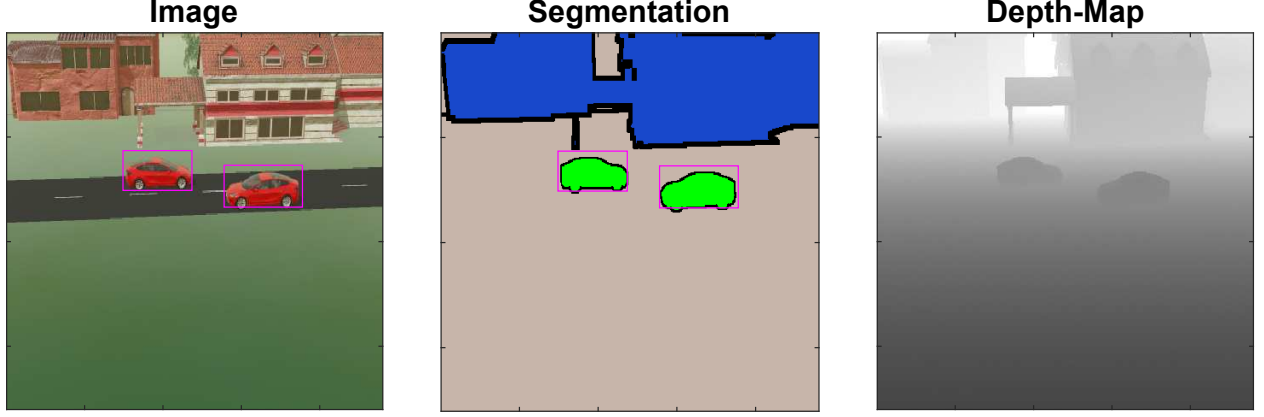


Figure 10. CVS information provided to each UAV by the sensors simulated by Webots

The control $u_{i,k}$ is a yaw angle increment taken in $\mathbb{U} = \{-\pi/18, -\pi/36, 0, \pi/36, \pi/18\}$. The prediction horizon of the MPC is set to $h = 12$. Nevertheless, only $u_{i,k}$ and $u_{i,k+h/2}$ are chosen freely in \mathbb{U} , then $u_{i,k+\tau} = u_{i,k}$ and $u_{i,k+h/2+\tau} = u_{i,k+h/2}$ for $\tau = 1, \dots, h/2 - 1$, i.e., the MPC is designed by computing only two values of the control, one at the beginning of the MPC and one at the middle of the prediction horizon. Moreover, to reduce computational burden, only the predicted FoV $\mathbb{F}(\mathbf{x}_{i,k+h/2|k}^{u,P})$ and $\mathbb{F}(\mathbf{x}_{i,k+h|k}^{u,P})$ are used in the MPC approach.

At time t_k , the MPC provides $\mathbf{x}_{i,k:h}^u$ to a low-level PID controller designed to ensure a constant speed module of $v^u = 5$ m/s and a constant fly height, higher than all obstacles and different for each UAV to avoid collision.

B. Evaluation metrics

The performance of the propose approach is evaluated considering the average surface of the set estimates of identified targets

$$\Phi_{i,k}^t = \frac{1}{\text{card}(\mathcal{L}_{i,k}^t)} \sum_{j \in \mathcal{L}_{i,k}^t} \phi(\mathbb{X}_{i,j,k}^t), \quad (63)$$

as well as the average localization error with respect to a point estimate taken as the barycenter $c(\mathbb{X}_{i,j,k}^t)$ of the set estimate

$$e_{i,k}^t = \frac{1}{\text{card}(\mathcal{L}_{i,k}^t)} \sum_{j \in \mathcal{L}_{i,k}^t} \|\mathbf{x}_{j,k}^{t,g} - c(\mathbb{X}_{i,j,k}^t)\|. \quad (64)$$

The theoretical coverage of the FoV of the UAVs at time k

$$\Phi_k^{\text{FoV}} = \phi\left(\bigcup_{i \in \mathcal{N}^u} (\mathbb{F}(\mathbf{x}_{i,k}^u) \cap \mathbb{X}_g)\right) \quad (65)$$

represents the part of \mathbb{X}_g observed at time t_k by all UAVs if there is no obstacle nor targets. The part of the ground that is actually seen and identified as ground at time t_k is

$$\Phi_k^g = \phi\left(\bigcup_{i \in \mathcal{N}^u} \mathbb{P}_i^g(\mathcal{Y}_{i,k}^g)\right). \quad (66)$$

The cumulated ground surface observed up to time t_k is

$$\Phi_{i,k}^{\text{Cg}} = \phi\left(\bigcup_{\tau=1}^k \bigcup_{i \in \mathcal{N}^u} \mathbb{P}_i^g(\mathcal{Y}_{i,\tau}^g)\right). \quad (67)$$

Most of these metrics may be expressed relative to the ground surface $\phi(\mathbb{X}_g)$.

Additional metrics of interest are the surface $\phi(\bar{\mathbb{X}}_{i,k}^t)$ of the set $\bar{\mathbb{X}}_{i,k}^t$, and the surface $\phi(\bar{\mathbb{X}}_{i,k}^t \cap \mathbb{X}_{i,k}^h)$ of the part of $\bar{\mathbb{X}}_{i,k}^t$ which has been occluded by an obstacle. In this last metric, the set $\mathbb{X}_{i,k}^h$ represents the portion of \mathbb{X}_g that has not been seen by UAV i at a previous time instant due to an occlusion by an obstacle and has not yet been observed again up to time t_k . This set is initialized with $\mathbb{X}_{i,0}^h = \emptyset$ and updated as

$$\mathbb{X}_{i,k|k}^h = (\mathbb{X}_{i,k-1}^h \cup \mathbb{H}_{i,k}) \setminus \mathbb{P}_{i,k}^g(\mathcal{Y}_{i,k}^g), \quad (68)$$

Moreover, using information received from its neighbors, UAV i updates $\mathbb{X}_{i,k|k}^h$ as

$$\mathbb{X}_{i,k}^h = \left(\bigcup_{\ell \in \mathcal{N}_{i,k}} \mathbb{X}_{\ell,k|k}^h \right) \setminus \left(\bigcup_{\ell \in \mathcal{N}_{i,k}} \mathbb{P}_{\ell,k}^g(\mathcal{Y}_{\ell,k}^g) \right). \quad (69)$$

C. Results

Results have been averaged over 10 independent simulations, each lasting 300 s. A video illustrating the evaluation of the set estimates for one simulation is available at: <https://nextcloud.centralesupelec.fr/s/Sxf5Nk2RJRXMyzk>.

Figure 11 shows the sets $\bar{\mathbb{X}}_{i,k}^t$ (in yellow), $\mathbb{X}_{i,j,k}^t$ (in green), $\mathbb{X}_{i,k}^o$ (in black), and $\mathbb{X}_{i,k}^h$ (in blue) for a typical realization at 4 time instants. Since there is no restriction on their communication range, all UAVs share the same set estimates.

Figure 12 (top) illustrates the evolution of $e_{i,k}^t$ (in red). Between $t = 150$ s and $t = 300$ s, the average target localization error $e_{i,k}^t$ evolves around 1.0 ± 0.4 m. Figure 12 (bottom) shows the evolution of the radius of a disc which area is $\Phi_{i,k}^t$. Between $t = 150$ s and $t = 300$ s, it is around 14 ± 5 m. This localization error remains small, but the uncertainty is relatively large. This is due to the fact that there are not enough UAVs to permanently observe the targets. In absence of observations, the uncertainty grows. Moreover, the absence of knowledge of the dynamics of targets (apart from their maximal velocity), does not enable UAVs to efficiently predict the evolution of the identified targets.

Figure 13 shows $\text{card}(\mathcal{L}_{i,k}^t)$, the cumulated number of detected targets (in red). The UAVs are able to identify all targets in less than 150 seconds. Figure 13 also shows the number of targets included in the FoV of all UAVs (in black) and the number of targets that are identified, *i.e.*, $\text{card}(\bigcup_{\ell \in \mathcal{N}^u} \mathcal{D}_{\ell,k}^t)$ (in blue). The difference comes from the obstacles hiding some targets, or targets located in the FoV, but too far away to be properly identified.

Figure 14 shows the evolution of $\phi(\bar{\mathbb{X}}_{i,k}^t)/\phi(\mathbb{X}_g)$ (in orange), of $\phi(\bar{\mathbb{X}}_{i,k}^t \cap \mathbb{X}_{i,k}^h)/\phi(\mathbb{X}_g)$ (in blue) and of $\Phi_{i,k}^{\text{Cg}}/\phi(\mathbb{X}_g)$ (in purple). One observes that $\phi(\bar{\mathbb{X}}_{i,k}^t)$ decreases quickly during the first time steps and remains around $26 \pm 3\%$ of $\phi(\mathbb{X}_g)$. As $\bar{\mathbb{X}}_{i,k}^t$ does not become empty, the fleet is unable to ensure that all targets have been found. The evolution of $\phi(\bar{\mathbb{X}}_{i,k}^t \cap \mathbb{X}_{i,k}^h)/\phi(\mathbb{X}_g)$ shows that after $t = 150$ s, almost two third of $\bar{\mathbb{X}}_{i,k}^t$ belongs to $\bar{\mathbb{X}}_{i,k}^t \cap \mathbb{X}_{i,k}^h$, and to parts of \mathbb{X}_g that have been hidden by obstacles. These parts of $\bar{\mathbb{X}}_{i,k}^t$ intersecting $\mathbb{X}_{i,k}^h$ grow until they are observed from a different point of view. This is clearly a limitation of the trajectory design approach, which is unable to determine the best point of view to observe some previously hidden areas.

$\Phi_{i,k}^{\text{Cg}}$ increases quickly at the beginning until all targets have been identified. After 150 s, $\Phi_{i,k}^{\text{Cg}}/\phi(\mathbb{X}_g)$ is above 90 % and reaches about 93 % at the end of the simulations. Since 5% of \mathbb{X}_g is occupied by obstacles, the maximum theoretical value of $\Phi_{i,k}^{\text{Cg}}/\phi(\mathbb{X}_g)$ is 95%. UAVs have explored nearly all the RoI. The remaining 2 % correspond

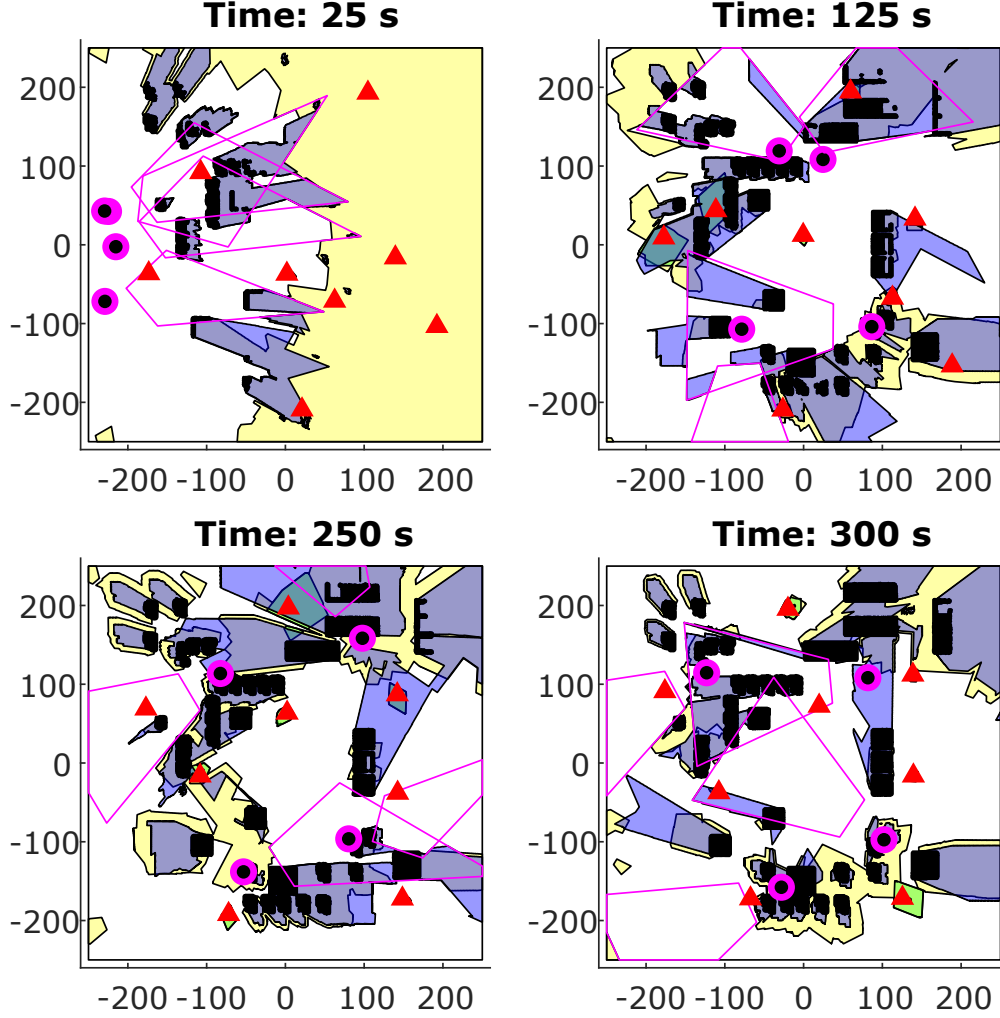


Figure 11. Set estimates $\mathbb{X}_{i,j,k}^t$ (green), $\mathbb{X}_{i,k}^t$ (yellow), $\mathbb{X}_{i,k}^o$ (black), and $\mathbb{X}_{i,k}^h$ (blue) at different time instant; The UAVs and the intersection of their FoV with the ground are represented in purple; Targets are represented by red triangles.

to areas around buildings located close to the borders of the RoI. This is a second issue of the trajectory design approach: the criterion (60) favors reduction of sets close to UAVs and does not impose the full exploration of the RoI.

Figure 15 illustrates the evolution of $\Phi_k^{\text{FoV}}/\phi(\mathbb{X}_g)$ and of $\Phi_k^g/\phi(\mathbb{X}_g)$. Initially, both quantities are small, as the UAVs are launched from the same location. Their FoVs intersect significantly. After few time steps, the UAVs are able to spread and at each time instant to monitor about 27% of the RoI. Due to the presence of obstacles, the effective ground area observed by the fleet reduces to about 18%. The oscillations of both curves are due to the update of the trajectories with a period of 3 s.

IX. CONCLUSION

This paper presents an approach to solve a CSAT problem in an unknown and cluttered environment with set-membership approach exploiting CVS information. For that purpose, several hypotheses related to the information

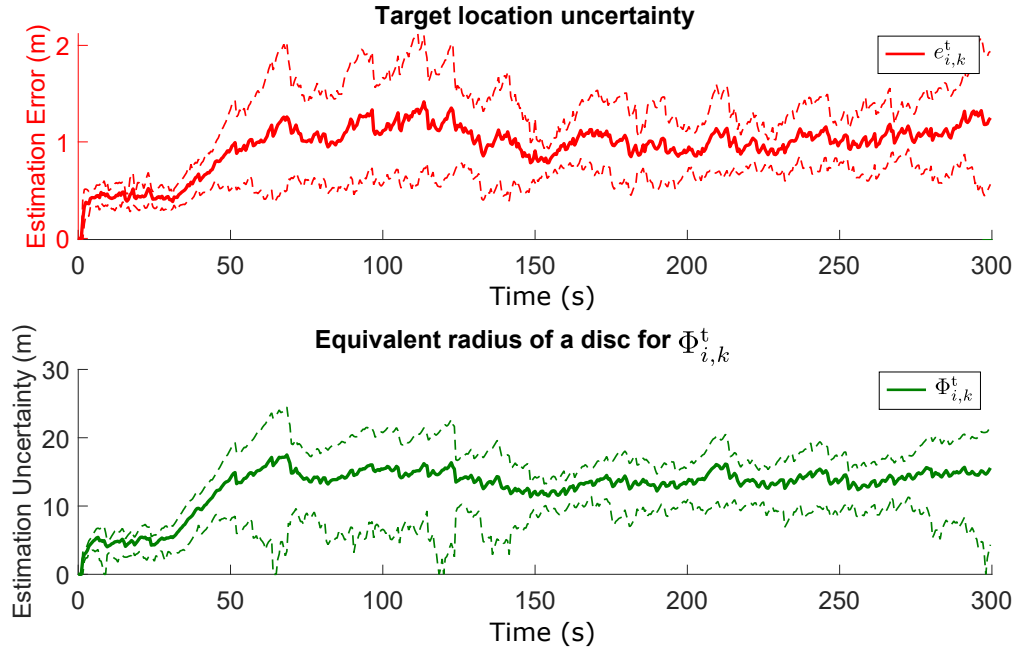


Figure 12. Mean value and standard deviation over 10 simulations of $e_{i,k}^t$ (top) and of the radius of a disc of the same area as $\Phi_{i,k}^t$ (bottom).

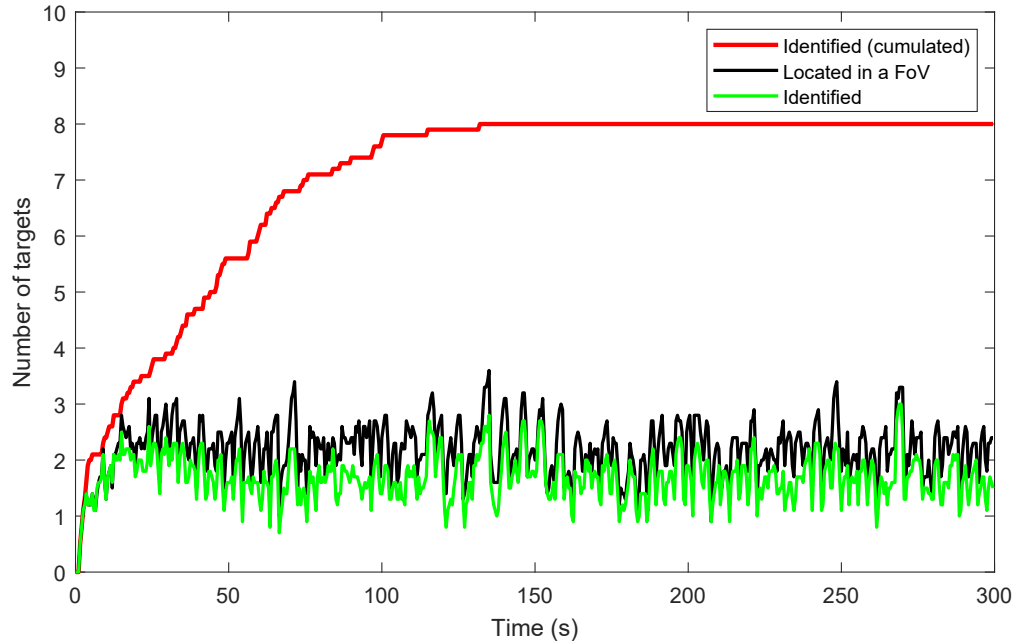


Figure 13. Evolution with time of $\text{card}(\mathcal{L}_{i,k}^t)$ (red), of the number of targets located in the FoV of at least one UAV (black), and of the number of identified targets, *i.e.*, of $\text{card}(\bigcup_{\ell \in \mathcal{N}^u} \mathcal{D}_{\ell,k}^t)$ (green).

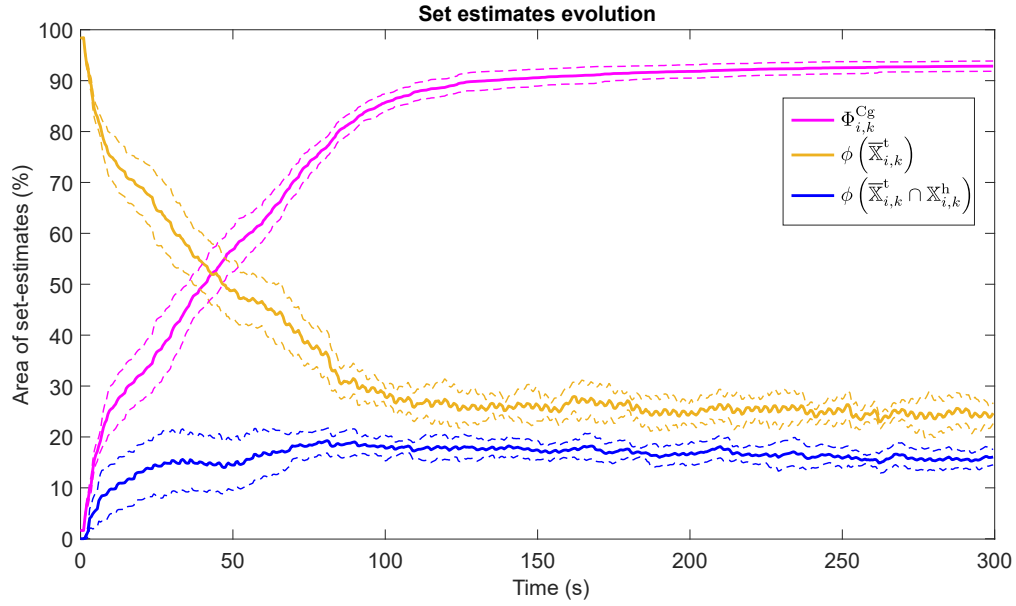


Figure 14. Top: mean value with standard deviation over 10 simulations of $\Phi_{i,k}^{Cg}$ (purple), $\phi(\bar{\mathbb{X}}_{i,k}^t)/\phi(\mathbb{X}_g)$ (orange), $\phi(\bar{\mathbb{X}}_{i,k}^t \cap \mathbb{X}_{i,k}^h)/\phi(\mathbb{X}_g)$ (blue).

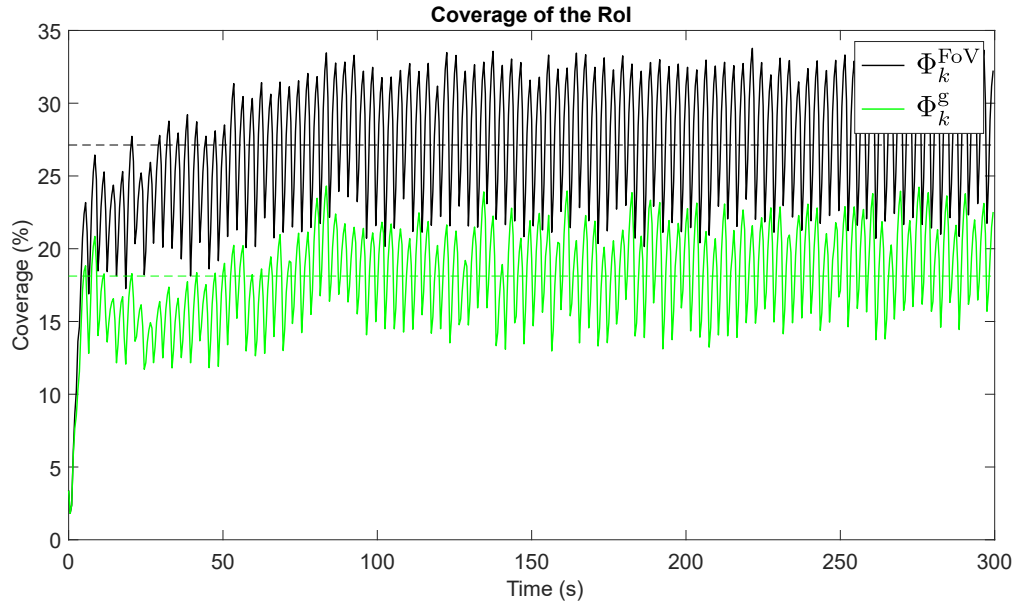


Figure 15. Mean value of $\Phi_k^{FoV}/\phi(\mathbb{X}_g)$ (black) and of $\Phi_k^g/\phi(\mathbb{X}_g)$ (green); the dashed lines represent the corresponding average over time.

provided by CVS are introduced to make such information exploitable by set-membership techniques. They consist mainly of a model for a depth measurements, and a model for the interpretation of the pixel classification.

Based on these hypotheses, CVS information is exploited by the proposed set-membership algorithm in each UAV to characterize sets guaranteed to contain the true location of identified targets and a set potentially containing the targets remaining to detect. The remainder of the RoI is proved to be free of targets. Via communications, the set-membership approach allows an easy exploitation of estimates provided the neighbors of each UAV to get refined estimates. Finally, each UAV updates its trajectory using a cooperative MPC approach.

Simulation results have shown the performance of the proposed set-membership CSAT algorithm considering a simplified urban environment. Some limitations have also been evidenced regarding the ability of the fleet to entirely explore the RoI and to observe area hidden by obstacles with the best point of view. These issues will be addressed in future work by building a 2.5D or a 3D map [62] of the environment during exploration. This will allow UAVs to predict the portions of the ground occluded by obstacles during their trajectory design. Other research directions may include the processing of decoys erroneously detected as targets by the CVS.

REFERENCES

- [1] C. Robin and S. Lacroix, "Multi-robot target detection and tracking: taxonomy and survey," *Autonomous Robots*, vol. 40, no. 4, pp. 729–760, 2016.
- [2] J. P. Queralta, J. Taipalmaa, B. C. Pullinen, V. K. Sarker, T. N. Gia, H. Tenhunen, M. Gabbouj, J. Raitoharju, and T. Westerlund, "Collaborative multi-robot search and rescue: Planning, coordination, perception, and active vision," *IEEE Access*, vol. 8, pp. 191617–191643, 2020.
- [3] S. S. Abood, K. Q. Hussein, and M. T. Gaata, "Survey on Modern Applications of Multiple Unmanned Aerial Vehicles (UAV) Systems," in *Proc. IEEE CSCIT*, pp. 179–184, IEEE, 2022.
- [4] M. Lyu, Y. Zhao, C. Huang, and H. Huang, "Unmanned aerial vehicles for search and rescue: A survey," *Remote Sensing*, vol. 15, no. 13, p. 3266, 2023.
- [5] J. Li, X. Zhai, J. Xu, and C. Li, "Target search algorithm for AUV based on real-time perception maps in unknown environment," *Machines*, vol. 9, no. 8, pp. 147–173, 2021.
- [6] Y. Ji, Y. Zhao, B. Chen, Z. Zhu, Y. Liu, H. Zhu, and S. Qiu, "Source searching in unknown obstructed environments through source estimation, target determination, and path planning," *Building and Environment*, vol. 221, pp. 109266–109306, 2022.
- [7] J. A. Placed, J. Strader, H. Carrillo, N. Atanasov, V. Indelman, L. Carlone, and J. A. Castellanos, "A survey on active simultaneous localization and mapping: State of the art and new frontiers," *IEEE Trans. Robotics*, vol. 39, no. 3, pp. 1686–1705, 2023.
- [8] M. J. Kuhlman, M. W. Otte, D. Sofge, and S. K. Gupta, "Multipass target search in natural environments," *Sensors*, vol. 17, no. 11, pp. 2514–2550, 2017.
- [9] X. Zhu, F. Vanegas, F. Gonzalez, and C. Sanderson, "A multi-UAV system for exploration and target finding in cluttered and GPS-denied environments," in *Proc. IEEE ICUAS*, pp. 721–729, 2021.
- [10] L. Zhao, R. Li, J. Han, and J. Zhang, "A distributed model predictive control-based method for multidifferent-target search in unknown environments," *IEEE Trans. Evol. Comput.*, vol. 27, no. 1, pp. 111–125, 2022.
- [11] J. Ibenhal, L. Meyer, H. Piet-Lahanier, and M. Kieffer, "Localization of Partially Hidden Moving Targets Using a Fleet of UAVs via Bounded-Error Estimation," *IEEE Trans. Robotics*, vol. 39, no. 6, pp. 4211–4229, 2023.
- [12] B. Zhang, X. Lin, Y. Zhu, J. Tian, and Z. Zhu, "Enhancing Multi-UAV Reconnaissance and Search Through Double Critic DDPG With Belief Probability Maps," *IEEE Trans. Intelligent Vehicles*, vol. 9, no. 2, pp. 3827–3842, 2024.
- [13] J. Ibenhal, M. Kieffer, L. Meyer, H. Piet-Lahanier, and S. Reynaud, "Bounded-error target localization and tracking using a fleet of UAVs," *Automatica*, vol. 132, pp. 109809–109824, 2021.
- [14] P. M. Dames, "Distributed multi-target search and tracking using the PHD filter," *Autonomous robots*, vol. 44, no. 3, pp. 673–689, 2020.

- [15] Y. Hou, J. Zhao, R. Zhang, X. Cheng, and L. Yang, "UAV Swarm Cooperative Target Search: A Multi-Agent Reinforcement Learning Approach," *IEEE Trans. Intelligent Vehicles*, vol. 9, no. 1, pp. 568–578, 2023.
- [16] A. Banerjee and J. Schneider, "Decentralized Multi-Agent Active Search and Tracking when Targets Outnumber Agents," *arXiv preprint arXiv:2401.03154*, 2024.
- [17] H. Tang, W. Sun, H. Yu, A. Lin, M. Xue, and Y. Song, "A novel hybrid algorithm based on PSO and FOA for target searching in unknown environments," *Applied Intelligence*, vol. 49, pp. 2603–2622, 2019.
- [18] F. Vanegas, D. Campbell, M. Eich, and F. Gonzalez, "UAV based target finding and tracking in GPS-denied and cluttered environments," in *Proc. IEEE IROS*, pp. 2307–2313, 2016.
- [19] A. Goldhoorn, A. Garrell, R. Alqu  azar, and A. Sanfeliu, "Searching and tracking people with cooperative mobile robots," *Autonomous Robots*, vol. 42, no. 4, pp. 739–759, 2018.
- [20] A. A. Meera, M. Popovic, A. Millane, and R. Siegwart, "Obstacle-aware adaptive informative path planning for uav-based target search," in *Proc. IEEE ICRA*, pp. 718–724, 2019.
- [21] L. Reboul, M. Kieffer, H. Piet-Lahanier, and S. Reynaud, "Cooperative guidance of a fleet of UAVs for multi-target discovery and tracking in presence of obstacles using a set membership approach," *IFAC-PapersOnLine*, vol. 52, no. 12, pp. 340–345, 2019.
- [22] G. Hardouin, J. Moras, F. Morbidi, J. Marzat, and E. M. Mouaddib, "Next-Best-View planning for surface reconstruction of large-scale 3D environments with multiple UAVs," in *Proc. IEEE IROS*, pp. 1567–1574, 2020.
- [23] A. Asgharivaskasi and N. Atanasov, "Semantic OcTree mapping and Shannon mutual information computation for robot exploration," *IEEE Trans. Robotics*, vol. 39, no. 3, pp. 1910–1928, 2023.
- [24] H. Zhang, C. Xie, H. Toriya, H. Shishido, and I. Kitahara, "Vehicle Localization in a Completed City-Scale 3D Scene Using Aerial Images and an On-Board Stereo Camera," *Remote Sensing*, vol. 15, no. 15, pp. 3871–3891, 2023.
- [25] N. Atanasov, B. Sankaran, J. Le Ny, G. J. Pappas, and K. Daniilidis, "Nonmyopic view planning for active object classification and pose estimation," *IEEE Trans. Robotics*, vol. 30, no. 5, pp. 1078–1090, 2014.
- [26] F. Zhong, S. Wang, Z. Zhang, and Y. Wang, "Detect-SLAM: Making object detection and SLAM mutually beneficial," in *IEEE WACV*, pp. 1001–1010, 2018.
- [27] S. Zhang, X. Zhang, T. Li, J. Yuan, and Y. Fang, "Fast active aerial exploration for traversable path finding of ground robots in unknown environments," *IEEE Trans. Instrum. Meas.*, vol. 71, pp. 1–13, 2022.
- [28] Q. Serdel, J. Marzat, and J. Moras, "SMaNa: Semantic Mapping and Navigation Architecture for Autonomous Robots," *Proc. ICINCO*, vol. 1, pp. 453–464, 2023.
- [29] J. Park and Y. Kim, "Stereo vision based collision avoidance of quadrotor UAV," in *Proc. ICCAS*, pp. 173–178, 2012.
- [30] H.-G. Jeon, J. Park, G. Choe, J. Park, Y. Bok, Y.-W. Tai, and I. So Kweon, "Accurate depth map estimation from a lenslet light field camera," in *Proc. IEEE CVPR*, pp. 1547–1555, 2015.
- [31] L. Madhuanand, F. Nex, and M. Y. Yang, "Self-supervised monocular depth estimation from oblique UAV videos," *ISPRS journal of photogrammetry and remote sensing*, vol. 176, pp. 1–14, 2021.
- [32] T. Shimada, H. Nishikawa, X. Kong, and H. Tomiyama, "Fast and High-Quality Monocular Depth Estimation with Optical Flow for Autonomous Drones," *Drones*, vol. 7, no. 2, pp. 134–151, 2023.
- [33] E. Grilli, F. Menna, and F. Remondino, "A review of point clouds segmentation and classification algorithms," *ISPRS Archives*, vol. 42, p. 339, 2017.
- [34] A. Howard, M. Sandler, G. Chu, L.-C. Chen, B. Chen, M. Tan, W. Wang, Y. Zhu, R. Pang, V. Vasudevan, and others, "Searching for mobilenetv3," in *Proc. IEEE/CVF ICCV*, pp. 1314–1324, 2019.
- [35] S. Minaee, Y. Boykov, F. Porikli, A. Plaza, N. Kehtarnavaz, and D. Terzopoulos, "Image segmentation using deep learning: A survey," *IEEE Trans. Pattern Anal. Mach. Intell.*, vol. 44, no. 7, pp. 3523–3542, 2021.
- [36] J. Redmon, S. Divvala, R. Girshick, and A. Farhadi, "You only look once: Unified, real-time object detection," in *Proc. IEEE CVPR*, pp. 779–788, 2016.
- [37] S. Minaeian, J. Liu, and Y.-J. Son, "Effective and efficient detection of moving targets from a UAV camera," *IEEE Trans. Intell. Transp. Syst.*, vol. 19, no. 2, pp. 497–506, 2018.
- [38] X. Luo, Y. Wu, and L. Zhao, "YOLOD: A target detection method for UAV aerial imagery," *Remote Sensing*, vol. 14, no. 14, p. 3240, 2022.
- [39] P. Jiang, D. Ergu, F. Liu, Y. Cai, and B. Ma, "A Review of Yolo algorithm developments," *Procedia computer science*, vol. 199, pp. 1066–1073, 2022.

- [40] S. Minaeian, J. Liu, and Y.-J. Son, "Vision-based target detection and localization via a team of cooperative UAV and UGVs," *IEEE Trans. Syst. Man. Cybern.*, vol. 46, no. 7, pp. 1005–1016, 2015.
- [41] J. Sun, B. Li, Y. Jiang, and C.-y. Wen, "A camera-based target detection and positioning UAV system for search and rescue (SAR) purposes," *Sensors*, vol. 16, no. 11, pp. 1778–1802, 2016.
- [42] X. Wang, J. Liu, and Q. Zhou, "Real-time multi-target localization from unmanned aerial vehicles," *Sensors*, vol. 17, no. 1, pp. 33–61, 2016.
- [43] Y. Liu, Q. Wang, H. Hu, and Y. He, "A novel real-time moving target tracking and path planning system for a quadrotor UAV in unknown unstructured outdoor scenes," *IEEE Trans. Syst. Man. Cybern.*, vol. 49, no. 11, pp. 2362–2372, 2018.
- [44] D. Liu, W. Bao, X. Zhu, B. Fei, Z. Xiao, and T. Men, "Vision-aware air-ground cooperative target localization for UAV and UGV," *Aerosp. Sci. Technol.*, vol. 124, pp. 107525–107540, 2022.
- [45] T. M. Di Gennaro and J. Waldmann, "Sensor Fusion with Asynchronous Decentralized Processing for 3D Target Tracking with a Wireless Camera Network," *Sensors*, vol. 23, no. 3, pp. 1194–1228, 2023.
- [46] I.-F. Kenmogne, V. Drevelle, and E. Marchand, "Cooperative localization of drones by using interval methods," *Acta Cybernetica*, pp. 1–16, 2019.
- [47] Y. Ajmera and S. P. Singh, "Autonomous UAV-based Target Search, Tracking and Following using Reinforcement Learning and YOLOFlow," in *IEEE SSR*, pp. 15–20, 2020.
- [48] Y. Liu, M. Xu, G. Jiang, X. Tong, J. Yun, Y. Liu, B. Chen, Y. Cao, N. Sun, and Z. Li, "Target localization in local dense mapping using RGBD SLAM and object detection," *Concurrency and Computation: Practice and Experience*, vol. 34, no. 4, p. e6655, 2022.
- [49] Z. Zeng, Y. Zhou, O. C. Jenkins, and K. Desingh, "Semantic mapping with simultaneous object detection and localization," in *Proc. IEEE IROS*, pp. 911–918, 2018.
- [50] C. Sahin, G. Garcia-Hernando, J. Sock, and T.-K. Kim, "A review on object pose recovery: from 3d bounding box detectors to full 6d pose estimators," *Image. Vision. Comput.*, vol. 96, p. 103898, 2020.
- [51] Z. Fan, Y. Zhu, Y. He, Q. Sun, H. Liu, and J. He, "Deep learning on monocular object pose detection and tracking: A comprehensive overview," *ACM Computing Surveys*, vol. 55, no. 4, pp. 1–40, 2022.
- [52] A. Mousavian, D. Anguelov, J. Flynn, and J. Kosecka, "3d bounding box estimation using deep learning and geometry," in *Pro. IEEE CVPR*, pp. 7074–7082, 2017.
- [53] Z. Zhen, Y. Chen, L. Wen, and B. Han, "An intelligent cooperative mission planning scheme of UAV swarm in uncertain dynamic environment," *Aerospace Science and Technology*, vol. 100, pp. 105826–105842, 2020.
- [54] B. Allik, "Tracking of multiple targets across distributed platforms with fov constraints," in *Proc. IEEE CDC*, pp. 6044–6049, 2019.
- [55] A. Symington, S. Waharte, S. Julier, and N. Trigoni, "Probabilistic target detection by camera-equipped UAVs," in *Proc. IEEE ICRA*, pp. 4076–4081, 2010.
- [56] T. Niedzielski, M. Jurecka, B. Mizinski, W. Pawul, and T. Motyl, "First successful rescue of a lost person using the human detection system: A case study from Beskid Niski (SE Poland)," *Remote Sensing*, vol. 13, no. 23, pp. 4903–4921, 2021.
- [57] E. Yanmaz, "Joint or decoupled optimization: Multi-UAV path planning for search and rescue," *Ad Hoc Networks*, vol. 138, pp. 103018–103031, 2023.
- [58] A. Singh, F. Ramos, H. D. Whyte, and W. J. Kaiser, "Modeling and decision making in spatio-temporal processes for environmental surveillance," in *Proc. IEEE ICRA*, pp. 5490–5497, 2010.
- [59] O. Faugeras, *Three-dimensional computer vision: a geometric viewpoint*. MIT press, 1993.
- [60] P. D. Christofides, R. Scatoloni, D. M. De La Pena, and J. Liu, "Distributed model predictive control: A tutorial review and future research directions," *Comput Chem Eng*, vol. 51, pp. 21–41, 2013.
- [61] Webots, "<http://www.cyberbotics.com>."
- [62] A. Souza and L. M. Gonçalves, "Occupancy-elevation grid: an alternative approach for robotic mapping and navigation," *Robotica*, vol. 34, no. 11, pp. 2592–2609, 2016.

APPENDIX

A. Characterization of $\mathbb{X}_{i,j}^{t,m}$ and \mathbb{X}_i^o

This section describes an approach to get an outer-approximation of the set estimate $\mathbb{X}_{i,j}^{t,m}$ introduced in Section V-A as well as an inner-approximation \mathbb{X}_i^o of the r^s -ground neighborhood of $\bigcup_{m \in \mathcal{N}^o} p_g(\mathbb{S}_m^o)$ introduced in Section V-B2. Both sets requires the characterization of $\mathbb{P}_i((n_r, n_c))$ defined in (35).

For any pixel (n_r, n_c) , the set $\mathbb{P}_i((n_r, n_c))$ is the intersection between (i) the half cone of apex \mathbf{x}_i^c and vertices corresponding to one of the four unit vectors $\mathbf{M}_{\mathcal{F}_i^c}^{\mathcal{F}_i^c} \mathbf{v}_\ell^{\mathcal{F}_i^c}$, $\ell = 1, \dots, 4$ with $\mathbf{v}_1^{\mathcal{F}_i^c} = \mathbf{v}^{\mathcal{F}_i^c}(n_c, n_r)$, $\mathbf{v}_2^{\mathcal{F}_i^c} = \mathbf{v}^{\mathcal{F}_i^c}(n_c, n_r - 1)$, $\mathbf{v}_3^{\mathcal{F}_i^c} = \mathbf{v}^{\mathcal{F}_i^c}(n_c - 1, n_r - 1)$, and $\mathbf{v}_4^{\mathcal{F}_i^c} = \mathbf{v}^{\mathcal{F}_i^c}(n_c, n_r - 1)$ and (ii) the space between the two spheres of center \mathbf{x}_i^c and radii $\frac{1}{1+\underline{w}} \mathbf{D}_i(n_r, n_c)$ and $\frac{1}{1+\underline{w}} \mathbf{D}_i(n_r, n_c)$. Figure 3 illustrates these four vectors $\mathbf{v}_\ell^{\mathcal{F}_i^c}$ which direction is represented by blue lines.

A truncated pyramidal outer-approximation $\bar{\mathbb{P}}_i((n_r, n_c))$ of $\mathbb{P}_i((n_r, n_c))$ is obtained considering the angles θ_ℓ between $\mathbf{v}^{\mathcal{F}_i^c}(n_c - 0.5, n_r - 0.5)$, the unit vector supporting the light-ray illuminating the center of the pixel and $\mathbf{v}_\ell^{\mathcal{F}_i^c}$, $\ell \in \{1, 2, 3, 4\}$. The eight vertices of $\bar{\mathbb{P}}_i((n_r, n_c))$ are then

$$\underline{\mathbf{x}}_\ell^p(n_r, n_c) = \mathbf{x}_i^c + \frac{1}{1+\underline{w}} \mathbf{D}_i(n_r, n_c) \mathbf{M}_{\mathcal{F}_i^c}^{\mathcal{F}_i^c} \mathbf{v}_\ell^{\mathcal{F}_i^c}, \quad (70)$$

$$\bar{\mathbf{x}}_\ell^p(n_r, n_c) = \mathbf{x}_i^c + \frac{1}{\cos(\theta_\ell)} \frac{1}{1+\underline{w}} \mathbf{D}_i(n_r, n_c) \mathbf{M}_{\mathcal{F}_i^c}^{\mathcal{F}_i^c} \mathbf{v}_\ell^{\mathcal{F}_i^c}, \quad (71)$$

with $\ell \in \{1, 2, 3, 4\}$.

Then, to evaluate $\mathbb{X}_{i,j}^{t,m}$ using (38), one determines

$$\mathbf{p}_g(\mathbb{P}_{i,j}^t) = \bigcap_{(n_r, n_c) \in [\mathcal{Y}_{i,j}^t] \cap \mathcal{Y}_i^t} \mathbf{p}_g(\mathbb{P}_i((n_r, n_c))) \quad (72)$$

$$\subset \bigcap_{(n_r, n_c) \in [\mathcal{Y}_{i,j}^t] \cap \mathcal{Y}_i^t} \mathbf{p}_g(\bar{\mathbb{P}}_i((n_r, n_c))), \quad (73)$$

as $\mathbb{P}_i((n_r, n_c)) \subset \bar{\mathbb{P}}_i((n_r, n_c))$. Since $\bar{\mathbb{P}}_i((n_r, n_c))$ is convex, an outer approximation of $\mathbf{p}_g(\mathbb{P}_i((n_r, n_c)))$ is obtained considering the convex hull $\bar{\mathbb{P}}_{g,i}((n_r, n_c))$ of $\mathcal{P}_{g,i}(n_r, n_c) = \{\mathbf{p}_g(\underline{\mathbf{x}}_\ell^p(n_r, n_c)), \mathbf{p}_g(\bar{\mathbf{x}}_\ell^p(n_r, n_c))\}_{\ell \in \{1 \dots 4\}}$. Finally, an outer-approximation of $\mathbb{X}_{i,j}^{t,m}$ is obtained as $\mathbb{X}_g \cap \left(\bigcup_{(n_r, n_c) \in [\mathcal{Y}_{i,j}^t] \cap \mathcal{Y}_i^t} \bar{\mathbb{P}}_{g,i}((n_r, n_c)) \oplus \mathbf{p}_g(\mathbb{C}^t(\mathbf{0})) \right)$.

One has $\mathbb{X}_i^o = \bigcup_{(n_r, n_c) \in \mathcal{Y}_i^o} \mathbb{S}^o((n_r, n_c), r^s)$, see (45). The definition 41 can be rewritten as

$$\mathbb{S}^o((n_r, n_c), r^s) = \bigcap_{\mathbf{x} \in \mathbf{p}_g(\mathbb{P}_i((n_r, n_c)))} \mathbb{D}_g(\mathbf{x}, r^s)$$

Since $\mathbb{P}_i((n_r, n_c)) \subset \bar{\mathbb{P}}_i((n_r, n_c))$, one has

$$\bigcap_{\mathbf{x} \in \mathbf{p}_g(\bar{\mathbb{P}}_i((n_r, n_c)))} \mathbb{D}_g(\mathbf{x}, r^s) \subset \bigcap_{\mathbf{x} \in \mathbf{p}_g(\mathbb{P}_i((n_r, n_c)))} \mathbb{D}_g(\mathbf{x}, r^s) \quad (74)$$

and

$$\bigcap_{\mathbf{x} \in \mathbf{p}_g(\bar{\mathbb{P}}_i((n_r, n_c)))} \mathbb{D}_g(\mathbf{x}, r^s) \subset \mathbb{S}^o((n_r, n_c), r^s). \quad (75)$$

Moreover, as $\bar{\mathbb{P}}_i((n_r, n_c))$ is convex,

$$\bigcap_{\mathbf{x} \in \mathbf{p}_g(\bar{\mathbb{P}}_i((n_r, n_c)))} \mathbb{D}_g(\mathbf{x}, r^s) = \bigcap_{\mathbf{x} \in \mathcal{P}_{g,i}(n_r, n_c)} \mathbb{D}_g(\mathbf{x}, r^s).$$

An inner approximation of $\mathbb{S}^o((n_r, n_c), r_s^{to})$ is then obtained as the intersection of, at most, eight discs each with a center in $\mathcal{P}_{g,i}(n_r, n_c)$ and of radius r^s . A convex polygon forming an inner-approximation of this intersection is then easily obtained. The set \mathbb{X}_i^o is then the union of the polygons obtained for each $(n_r, n_c) \in \mathcal{Y}_i^o$.

B. Characterization of $\mathbb{P}_i^g(\mathcal{Y}_i^g)$ and \mathbb{H}_i^g

To evaluate $\mathbb{P}_i^g(\mathcal{Y}_i^g)$ introduced in (40), the union of sets $\mathbb{P}_i^g((n_r, n_c))$ for $(n_r, n_c) \in \mathcal{Y}_i^g$ has to be characterized. Neglecting the limitation of the FoV by $\mathbb{B}(\mathbf{x}_i^u, d_{\max})$ and as \mathbb{X}_g is a part of a plane, $\mathbb{P}_i^g((n_r, n_c))$ is the convex quadrangle defined by the intersection of \mathbb{X}_g with the half-cone of apex \mathbf{x}_i^c and edges related to the four unit vector $\mathbf{v}_\ell^{\mathcal{F}_i^c}$, with $\ell = 1, \dots, 4$, see Figure 3. $\mathbb{P}_i^g(\mathcal{Y}_i^g)$ is then the union of the convex quadrangles $\mathbb{P}_i^g((n_r, n_c))$ for all $(n_r, n_c) \in \mathcal{Y}_i^g$.

Similarly, \mathbb{H}_i^g is the union of the convex quadrangles $\mathbb{P}_i^g((n_r, n_c))$ for all $(n_r, n_c) \in \mathcal{Y}_i^o \cup \mathcal{Y}_i^t \cup \mathcal{Y}_i^n$.